Selective lead (II) sorption using aminophosphonate-based sorbents: Effect of amine linker, characterization and sorption performance

Rana Neiber, Ahmed Galhoum, Ibrahim El-Tantawy El Sayed, Guibal Eric, Jiayu Xin, Xingmei Lu

Selective lead (II) sorption using aminophosphonate-based sorbents: Effect of amine linker, characterization and sorption performance

Rana R. Neiber [a,b,c], Ahmed A. Galhoum [d,*], Ibrahim El-Tantawy El Sayed [e,*], Eric Guibal [f], Jiayu Xin [a,c,g,h], Xingmei Lu [a,c,g,h,i,*]

[a] *Beijing Key Laboratory of Ionic Liquids Clean Process, CAS Key Laboratory of Green, Process, and Engineering, Institute of Process Engineering, Chinese Academy of Sciences, 100190 Beijing, China*
[b] *College of Chemical Engineering, University of Chinese Academy of Sciences, 19 A Yuquan Road, Beijing 100049, China*
[c] *School of Chemistry and Chemical Engineering, University of Chinese Academy of Sciences, 100049 Beijing, China*
[d] *Nuclear Materials Authority, P.O. Box 530, El-Maadi, Cairo, Egypt*
[e] *Chemistry Department, Faculty of Science, Menoufia University, Shebin El-Kom, Egypt*
[f] *Institut Mines Telecom – Mines Alès, C2MA, 6 avenue de Clavières, F-30319 Alès cedex, France*
[g] *Innovation Academy for Green Manufacture, Chinese Academy of Sciences, Beijing 100190, China*
[h] *Dalian National Laboratory for Clean Energy, Dalian 116023, China*
[i] *Department of Chemistry, University of Chinese Academy of Sciences, 100049, Beijing, China*

ABSTRACT

A one-pot synthesis procedure is designed for preparing two α-aminophosphonate-based-sorbents (DA and TA sorbents). The reaction takes place between amine precursors (two different aliphatic amines with different chain lengths and amino group content; i.e., ethylenediamine (DA) or diethylenetriamine (TA), respectively) and both salicylaldehyde and diphenyl phosphite. Ionic liquid may be used under controlled conditions as an alternative to $TiCl_4$ catalyst. These materials are first characterized by SEM-EDX, AFM, BET, XRD, FTIR, ^{1}H-, ^{13}C-, and ^{31}P NMR, XPS, TGA, elemental analysis (CHNP), and titration (PZC). Combined with the study of pH effect on Pb(II) sorption, FTIR and XPS analyses are used for exploring the mechanisms involved in metal binding. In a second step, the sorption properties are compared for Pb(II) recovery at pH ≈5. Maximum sorption is influenced by the length of the chain: DA (0.694 mmol Pb g^{-1}) > TA (0.494 mmol Pb g^{-1}). The sorption isotherms are modelled by the Sips equation for DA (and the Langmuir Dual Site equation) and by the Langmuir equation for TA. Ther-modynamic parameters (ΔG°, ΔH° and ΔS°) indicate the spontaneous, endothermic nature and randomness increases during the sorption process. The uptake kinetics (equilibrium reached ≈120 min) is almost equally fitted by the pseudo-first-order rate equation and the pseudo-second-order rate equation. The sorbents show selective Pb(II) sorption against heavy base metals in multi-component solutions. QSAR tools (quantitative ac-tivity structure–activity relationships) are used for evaluating the correlation between their intrinsic metal characteristics and their affinities for sorbents. The sorbents are efficiently recycled for at least 5 cycles using 0.2 M HCl as the eluent (loss in sorption and desorption performances ≈10-14% at the fifth cycle, compared with the first cycle).

1. Introduction

Heavy metals' contamination of the aquatic environment is a major concern worldwide. Their harmfulness is due to their persistence and long-lasting effects on the ecosystems [1,2]. The contamination of industrial wastewater by heavy metals is one of the major environmental problems: in addition to naturogenic sources (weathering of ores and natural drainage of soils), mining and metallurgical industries generate important contamination flux for the aquatic resources. Lead (Pb) is one of the most widely scattered hazardous and toxic metals released into the soil and water bodies in the world because of increasing human activity, industrial and urban activities, e.g., metal smelting, coal

---

* Corresponding authors at: Beijing Key Laboratory of Ionic Liquids Clean Process, CAS Key Laboratory of Green, Process, and Engineering, Institute of Process Engineering, Chinese Academy of Sciences, 100190 Beijing, China; Department of Chemistry, University of Chinese Academy of Sciences, 100049, Beijing, China
E-mail addresses: galhoum_nma@yahoo.com (A.A. Galhoum), ibrahimtantawy@yahoo.co.uk (I. El-Tantawy El Sayed), xmlu@ipe.ac.cn (X. Lu).

burning, gasoline consumption, lead–acid batteries, paints, and other solid waste releases [3–6]. The toxicity of heavy metal ions in water is mainly associated with their ready accumulation in the food chain. Therefore, removing metal ions from contaminated water bodies is a strategic issue for human health, living organisms, and the environment [1–3,7]. Metal ions can be removed from aqueous solutions (leachates and hydrometallurgical streams) using precipitation, solvent extraction, impregnated resins; however, sorption processes are frequently considered more efficient for treating dilute effluents; due to their environmental friendliness and high efficiency [1–6]. To date, the most often used sorbents for the separation of lead ions are carbon-based sorbents [8], synthetic and natural polymers [3], metal organic frameworks (MOFs) [4,9], chelating and ion-exchange resins [10–12], as well as composite [5,6,8,13]. Additional benefits may also consist of valorizing wastes and the recycling of metals, as suggested by many national and regional regulations [14–16].

The multi-functionality of resins is frequently considered a good strategy for designing sorbents to improve sorption performance and metal selectivity [17–21]. Alexandratos's Group theorized the different benefits or effects the bi-functionality can bring for metal sorption and selectivity criterion: intra-ligand cooperation, recognition ligand, hydrophilic effect, acid-base properties, etc. [22,23]. Reactivity of resins may be changed through the grafting of new types of functional groups such as amino groups, alone or in combination with phosphonate groups (i.e., salt/ester) through aminophosphonate, and as carboxyl groups, alone or in combination with amine groups through ethylenediaminetetraacetic acid (DETA) [5,8], or amino-acids [21,24]. More specifically, organophosphorus compounds and their derivatives are good metal complexing agents with numerous applications in water treatment, metal extraction, or pollution control [19,25,26]. The multifunctional materials offer the possibility to improve the sorption capacities (increased density of reactive groups), the selectivity (synergistic effect of vicinal functions), and the pH range for efficient sorption [20,27–29]. Previously, some aminophosphonate derivatives were synthesized and tested for the binding of uranium [19,28], rare earth [25], and cadmium [29]. Two α-aminophosphonate derivatives of chitosan were produced by playing with methyl- vs. phenyl-substitution [28]. The comparison of sorption performances allowed illustrating the impact of donor groups on the orientation and enhancement of sorption performances: methyl-derivative being more efficient, probably because of lower steric hindrance, acid-base properties, and donor/acceptor effect of the substituent. The structure/activity relationship was also illustrated by investigating the impact of inserted groups (carboxylic vs. amine) onto uranium sorption [19]: the presence of amine and carboxylic groups onto the precursor of the aminophosphonate resin decreases sorption performance and may affect the thermodynamics of the system. Aminophosphonate-based materials have already been reported as efficient sorbents for lead recovery. These modifications may involve grafting of reactive moieties onto titanium oxide [30], zirconium [31], apatite [32]. Commercial resins bearing aminophosphonate groups were also used for lead sorption [33,34]. However, the two-step preparation of these composite adsorbent, certainly increase the time and cost of the process. In this regard, the preparation of aminophosphonate derivatives by one-pot synthesis strategy and its utilization for selective Pb(II) adsorption from aqueous media could be effective.

This study focuses on synthesizing two new α-aminophosphonate-based sorbents using a one-pot synthesis procedure by direct reaction between amine precursors (e.g., ethylenediamine and diethylenetriamine) with salicylaldehyde and diphenyl phosphite. Our previous investigations have shown the importance of the environment of phosphonate groups on their reactivity for metal sorption. This is the reason for extending this research to other modifications of this environment to enrich the understanding of these effects and contribute to the optimization of aminophosphonate-based sorbents. The effect of the environment may be exerted through the inductive effect of

substituents, hydrophilic behavior, and acid-base characteristics. This specific contribution brings complementary information on the effect of the length of amine chain on the sorption properties in terms of sorption criteria (uptake kinetics and sorption isotherms) as well as on separation criteria. The simple and environmentally-friendly alternative method (involving ionic liquid as an eco-friendly catalyst instead of a hazardous one) is another breaking contribution. Associated with extensive characterization of materials, those conjunctions of studies contribute to a complete and innovative approach. The physicochemical structure and properties are first characterized by elemental analysis, FTIR, XPS, NMR analysis (including ^{1}H, ^{13}C, and ^{31}P), BET, SEM-EDX, TGA, AFM, and PZC. In a second step, the sorption properties of these two sorbents are compared by studying parameters such as pH, uptake kinetics, sorption isotherms (including thermodynamic characterization). The recycling of the sorbents is investigated along with five cycles of sorption and desorption, using HCl solutions (0.2 M) as the eluent. To evaluate the selectivity of the sorbents for Pb(II), complementary experiments were performed using multi-component equimolar solutions (Co, Ni, Zn, Cd, in addition to Pb). The prepared DA and TA could be regarded as potential adsorbents for efficient removal of Pb(II) from aqueous media.

2. Materials and methods

2.1. Materials

Diethylenetriamine, ethylenediamine, diphenyl phosphite, and lead (II) chloride (99.5%), NiCl$_2$ (99%), CoCl$_2$ (99.7%) were supplied by Macklin (Beijing, China). Salicylaldehyde, ionic liquid (IL: pyridinium trifluoromethanesulfonate), ZnCl$_2$ (98%), CdCl$_2$ (99.99%), and acetonitrile were obtained from Aladdin (Beijing, China). Stock Pb(II) solutions were prepared by dissolving PbCl$_2$ salt, under heating, in demineralized water (concentration of the stock solution: 1 g Pb L^{-1}). All other chemicals were obtained from Prolabo products; they were used as received. Titanium tetrachloride (TiCl$_4$, 99.99%) was purchased from Shanghai Macklin Biochemical Co., Ltd. (Shanghai, China).

2.2. Synthesis of materials

Scheme 1 shows the synthesis route for the preparation of the sorbents, and gives their suggested structures. Salicylaldehyde (2 mmol), amine (either diamine or triamine) (1 mmol), and diphenyl phosphite (2 mmol). The mixture molar ratio (2:1:2) was stirred at room temperature for 10 min before dropping the IL Lewis acid catalyst (20% wt. percent of the total mixture weight). The mixture was stirred at room temperature for 3 days [19,28]. An alternative method (less environmentally friendly) consisted of using TiCl$_4$/CH$_3$CN (in an ice bath) as the catalytic system; the reaction took place in this case within 15 min. The final products were collected by filtration, washed with acetonitrile, and then air-dried to produce the corresponding α-aminophosphonate derivatives as a DA-based and TA-based sorbents. To purify the materials, the solids were recrystallized after being dispersed in chloroform or ethanol. Finally, the dried powders were stored in a desiccator before use. The comparative analysis of the products obtained through the two catalytic pathways (IL- and TiCl$_4$ routes) revealed that they are identical: physical characterization, spectroscopic data, and thin-layer chromatography (TLC) confirm the similarities in the final products. In addition, independently of the reaction time, the two routes reach the same reaction yield (remarkably efficient in terms of α-aminophosphonation). The reaction progress was monitored by thin-layer chromatography (TLC) using hexane and dichloromethane (3:1) until complete consumption of starting materials. The IL-route allows greener synthesis conditions while using IL as an eco-friendly catalyst.

2.3. Characterization of materials

The elemental analysis (C, H, N) was determined using an automatic
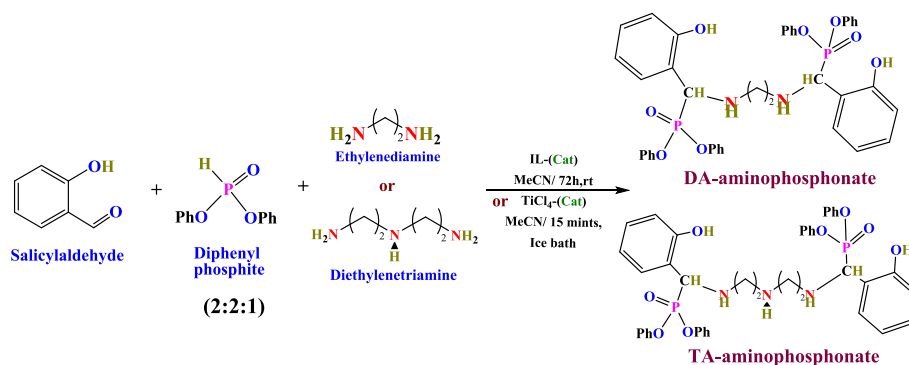
Scheme 1. Schematic route for the synthesis of α-aminophosphonate derivatives (DA and TA) (the scheme illustrates the reaction mechanism for both TiCl₄ catalysis and Ionic Liquid (IL) processes) and the expected structure of sorbents.

analyzer (CHNS Vario EL III-elementar analyzer, Elementar, Hanau, Germany). The determination of phosphorus content was obtained in a two-steps procedure. First, the sorbent was digested in concentrated HNO_3 solution ($\approx$68%) using a microwave digestion system (CEM MARS 6TM, CEM Corporation, Mattews, NC, USA) at 180 °C for 4 h. The mineralized solution was analyzed in a second step by ICP-AES (inductively coupled plasma atomic emission spectrometry, Agilent 5100, Santa Clara, CA, USA). The FTIR spectra (after preparing KBr pellet discs) were collected using a ThermoFisher Nicolet IS10 (Thermo Fisher Instruments, Waltham, MA, USA spectrometer). ^{1}H NMR 600 MHz, ^{13}C NMR 150 MHz, and ^{31}P NMR 243 MHz spectra were recorded in DMSO-d_6 using a Bruker Avance III HD 600 MHz NMR spectrometer–probe: BBFO cryoprobe (Bruker Biospin, Zurich, Switzerland). X-ray Photoelectron spectra were collected using a K-Alpha XPS system (ESCALAB 250Xi, Thermo Fisher Scientific, Waltham, USA); binding energies were calibrated to concerning C 1 s signal (adv. C at 284.8 eV). The Brunauer–Emmett–Teller (BET) surface areas and the Barett-Joyner-Halenda (BJH) adsorption model for pore size distributions of the sorbents were determined using an ASAP 2460, Version 2.01 surface area and porosity analyzer (Micromeritics Instrument Corporation, Norcross, GA, USA). For BET measurements, the sample was degassed at 60 °C for 6 h. Atomic force microscopy (AFM) images were acquired using a Brooke MultiMode 8 Probe: SNL-10, parameters: sharpened, k = 0.24 N/m, Al reflex coating (Brooke Corporation, Mannheim, Germany). Scanning electron microscopy (SEM) images were performed using a JEOL JSM-7800 Prime (JEOL Ltd., Tokyo, Japan). TG/DTA had been carried out using a thermogravimetric and differential thermal analyzer EXSTAR 6000, TG/DTA 6300 N (Seiko Instruments Inc. (SII), Tokyo, Japan), under N_2/O_2 atmosphere, within the temperature range 25–1000 °C and at the ramp rate of 10 °C/min. X-ray diffraction patterns were acquired using a SmartLab 9 diffractometer (Rigaku Corporation, Tokyo, Japan).

2.4. Metal sorption and desorption

The study of sorption performance was carried out in batch reactor at room temperature (i.e., 25 ± 1 °C, unless specified) under agitation (v: 150 rpm); in most cases, the sorbent dose (SD = m/V, where m is the amount of sorbent, g; and L is the volume of solution, L) was fixed to 0.5 g L^{-1}. For the study of the pH effect, the solution (initial concentration, C_0: 0.241 mmol Pb L^{-1}) with pH$_0$ (initial pH) varying between 2 and 9, was mixed for 10 h. The solutions were filtered using 1.2 μm pore size membranes. Notably, the solutions were not buffered; however, the equilibrium pH (pH$_{eq}$) was systematically monitored to correlate sorption performance with true pH value. The residual metal concentration in the filtrate (C$_{eq}$, mmol L^{-1}) was analyzed using ICP-AES (Multitype ICPE −9000, Shimadzu Corporation, Kyoto, Japan). The sorption capacity (q$_{eq}$, mmol g^{-1}) was calculated according to the mass balance equation: q$_{eq}$=(C$_0$ − C$_{eq}$)V/m. Sorption isotherms were obtained at

room temperature and pH$_0$: 5.0; initial metal concentration varied from 0.0724 to 2.413 mmol Pb L^{-1}. The residual concentrations (after the filtration of samples collected after 2 h of contact) were analyzed for calculating the equilibrium sorption capacities according to the mass balance equation and plotting the sorption isotherms (i.e., q$_{eq}$ = f(C$_{eq}$)). Uptake kinetics were performed by contact of samples with varying contact time for a sorbent dosage of 0.5 g L^{-1}; after filtration and analysis, the kinetic profile was plotted. Specific experimental conditions are systematically reported in the caption of the figures.

The investigation of sorption selectivity was performed using the same procedure with multi-component equimolar solutions (C$_0$: 1 mmol L^{-1}); competitor metals were selected among the metals usually present in the effluents of battery factories (i.e., Co, Ni, Cd, Zn). Standard experimental conditions have been selected: pH$_0$ = 5, SD = 0.5 g L^{-1}, time = 120 min, T = 25 ± 2 °C, v = 150 rpm.

Hydrochloric acid (0.2 M) was selected as the eluent to study metal desorption. The contact time between the eluent and the metal-loaded sorbent was set to 1 h (under constant agitation). The sorption and desorption performances were compared for five successive cycles. The desorption efficiency (DE) and regeneration rate (RR) were calculated according to the following equation:

$$DE = \frac{C_d \times V \times 100}{q_d \times m_d} \tag{1}$$

$$RR = \frac{q_d \times 100}{q_e} \tag{2}$$

where C$_d$ (mmol Pb L^{-1}) is the metal ion concentration in desorption solution, V(L) the volume of the desorption solution, q$_d$ (mmol Pb g^{-1}) the sorption capacity for metal-loaded material before desorption, q$_e$ (mmol Pb g^{-1}) is the sorption capacity at the first cycle, and m$_d$ (g) is the amount of the sorbent.

The modeling of uptake kinetics and sorption isotherms was performed using conventional models:

(a) uptake kinetics: pseudo-first and pseudo-second order rate equations, and the Crank equation (for simulating intraparticle diffusion),
(b) sorption isotherms: Langmuir, Freundlich, Sips, Temkin, and Dubinin-Raduskevich equations.

The relevant equations are reported in Tables S1a and S1b, respectively (see Supplementary Information). The determination of the model parameters was performed using the Mathematica® facilities for non-linear regression. The quality of the fit was calculated using the determination coefficient (i.e., R^2) and the Akaike Information Criterion (i.e., AIC, see Table S1).

The sorption tests were duplicated, and the relevant data are reported to show good reproducibility in sorption performances. In

addition, the repeatability in synthesis was tested with similar characterizations (available on-demand) and binding performances.

3. Results and discussion

3.1. Synthesis and characterization of new aminophosphonate materials

Scheme 1 illustrates the synthesis route for the preparation of α-aminophosphonates with different amine chains. This simple one-pot reaction occurs between amine (either diamine or triamine), salicylaldehyde, and diphenyl phosphite; IL is used as the catalyst (CH_3CN, 1 mL) for the production of sorbents (with tentative structures represented in Scheme 1). Scheme S1 (see Supplementary Information) shows the suggested mechanisms for the molecular interactions between the reagents for producing DA sorbent (diamine precursor); the synthesis of TA sorbent (triamine precursor) follows the same mechanisms. The first step consists of forming an imine-intermediate, followed by the attack of this intermediate by the electron-rich source of phosphorus, as nucleophilic phosphite, on the imine carbon atom (leading to the formation of phosphonium ion). This reaction is catalyzed by the IL Lewis acid catalyst (alternatively, $TiCl_4$ in acetonitrile can be used for processing the reaction, in a less environmentally friendly mode). In the last step of the process, the reaction of phosphonium intermediates with water promotes the elimination of phenol and the formation of the relevant α-aminophosphonates (Scheme S1) [19]. This interpretation of sorbent synthesis is supported by a series of analyses (see below). Based on the quantities of reagents and the effective amounts of products synthesized it was possible to evaluate the yields to (a) 67.32% for DA (i.e., 7.2 g for 10.70 g; the limiting agent is salicylaldehyde), and (b) 59.87% for TA (i. e., 4.52 g for 7.55 g; in this case, the limiting agent is diphenyl phosphite). The alternative route (using $TiCl_4$ as the catalyst, with faster synthesis kinetics but less environmental-friendly) produces comparable materials with slightly reduced yields: 5.12 g for TA and 8.16 g for DA (corresponding to yield decrease of 5.2% and 5.6%, respectively).

3.2. Characterization

3.2.1. Sorbent morphology and semi-quantitative analysis: SEM, SEM-EDX, AFM, and XRD analyses

SEM micrographs were analyzed with an image analyzer software to determine particle size distribution (Figure S1, see Supplementary Information). These data were collected using the functionalities of Foxit Phantom PDF for measuring tool distances and Origin 2018 for building histograms. The two sorbents have similar average size, but TA is more heterogeneous in size; d_P: 32.6 ± 9.4 μm for DA and 34.7 ± 13.7 μm for TA.

The morphology of the materials is characterized by SEM (Figures S2 and S3). DA and TA sorbents particles appear as irregular objects with irregular distribution in size (from approximately 10 μm to 100 μm) and granular surfaces. The sorbents show appreciable rough and porous surfaces; these properties are of critical importance for sorption processes while developing large specific surface areas and allowing water and metal ion transfer. The surface of the sorbents is significantly changed after lead sorption: apparently, lead is distributed over the whole surface of the sorbents. The loaded SEM images after sorption show that Pb(II) ions covered the caves, pores, and surfaces of sorbents. Table S2 shows the semi-quantitative EDX analysis of the surface of the sorbents before and after metal sorption. The semi-quantitative analysis is limited to a penetration depth corresponding to a fraction of the wavelength of the incident electron beam. The EDX spectra (not shown) confirms the presence of P element (K_α P signal, at 2.01 keV) and the appearance of a small peak (with poor sensitivity for K_α N signal at 0.392 keV), which confirm the phosphonomethylation of the polymers. The peaks for O $k_{\alpha 1}$ and C k_α are identified at energies of 0.525 keV and 0.277 keV, respectively [35]. Nitrogen content in TA is slightly higher than DA sorbent, consistently with the theoretical values given by elemental analysis (see below). The cartographies of elements at the surface of sorbent particles before and after metal sorption (not presented) show a great homogeneity in the distribution of both constitutive elements (i.e., C, N, P, and O) and sorbed Pb.

A semi-quantitative analysis was also performed on metal-loaded sorbents (Table S2). The EDX analysis clearly shows the appearance of $M_{\alpha 1}$ Pb signal (at 2.346 keV) and weak peaks of L_1 and $L_{\alpha 2,1}$ at around 9.185 keV and 10.551, respectively (not shown). The mass fractions of Pb are 18.52 % (w/w) and 8.59 % (w/w) for DA and TA sorbents, respectively. These data give preliminary information on the relatively higher affinity of the DA for Pb(II) than TA. Phosphorus and nitrogen contents after metal sorption decrease; due to a combination of screening effects, decrease in their relative fraction, associated with poor detection.

Atomic force microscopy (AFM) is a useful tool for analyzing the topography of sorbents. Figure S3 shows the 2-D and 3-D images of the surface of DA and TA sorbents before and after Pb(II) sorption. The roughness of the surface changes with metal binding. This significant change in the morphology for both DA and TA after Pb(II) sorption indicates that Pb(II) is well sorbed; apparently, the coating is homogeneous at the surface of the sorbents. This homogeneous surface modification is consistent with SEM observations.

X-ray diffraction analysis shows considerable change in the shape of the patterns (Figure S5a). Both DA and TA sorbents show poorly resolved peaks that demonstrate that the material is globally amorphous [36]. Broad bands are identified on raw materials (before Pb(II) sorption), in the range 2θ: 20-25°, which can be associated with inter- and intramolecular hydrogen bonds. After Pb(II) sorption, the broad diffraction peak is shifted from 2θ: ≈22.5° to 2θ: ≈26.4° in the case of TA. In the case of DA, the XRD pattern is entirely different with the appearance of a crystalline structure illustrated by sharp peaks at 2θ: 24.43°, 29.04°, and 35.00°; accounting for PbCl-based species [37]. In addition, four other peaks are identified at 5.80°, 17.2°, 20.0°, and 25.7°. The repetition of XRD analysis confirms that these differences in the profiles (especially after Pb(II) sorption) are meaningful between DA and TA. In addition, the small-angle diffraction X-ray analysis (SAED) of the two materials after lead sorption confirms the higher crystallinity of DA sorbent (compared with TA, Figure S5b) It is difficult finding a convincing explanation for the new peaks observed on the DA XRD pattern after metal binding. The higher density of amine groups in TA (compared with DA) may cause a weaker (unstable) chelation of the metal onto DA, which, in turn, could cause local precipitation of lead as PbO and then an increase in crystallinity.

3.2.2. Textural characterization – BET analysis

The textural characteristics of the two sorbents (before and after metal sorption) have been analyzed by N_2 sorption and desorption isotherms (Figure S6). The specific surface area (S_{BET}) of DA and TA sorbents are close to 6 m^2 g^{-1}. Surprisingly, S_{BET} drastically increases after Pb(II) sorption up to 40.3 and 37.6 m^2 g^{-1} for DA and TA, respectively. The coating of the internal surface and the accumulation of metal ions into the smallest micropores may increase the average pore size of the sorbents (as observed in Figure S6). One would expect the S_{BET} value to decrease with this clogging of the smallest pores and internal surface coating. Unexpectedly, a reciprocal trend is observed. The SEM and AFM figures showed a relative increase in the roughness of the surface of the sorbents that could partially explain the significant increase in specific surface area. Other explanation may refer to the effects of polymer swelling during the sorption step and to the expansion of the porous network due to the intercalation of metal ions (into the interlayer pores). This may also contribute to creating new pores and pockets with sponge-like structures and inter distant pores as the consequence of Pb(II) co-ordination with reactive groups held on the DA and TA internal network and at the sorbent surface. Similar properties have been reported for increasing the sorption efficiency of arsenate anions onto Cu(II)-loaded modified cellulose [38]. This hypothesis is corroborated by the

increased roughness of the sorbent surface [39], as confirmed by comparing SEM images (Figure S2 and S3). It is noteworthy that this phenomenon caused the formation of 2D nanosheets layers of few 100 nm in width and less than 100 nm thickness as visualized and highlighted in high magnification SEM panels. The high specific surface area after metal binding may result from this wide diversity of mechanisms. It is noticeable that this surface expansion is more important than the phenomena reported in the literature.

The pore volume (determined by the BJH method) is about two times larger for DA than for TA: despite the longer chain of the amine precursor in TA, the polymer obtained at the end of the synthesis is more compact. After metal sorption, the porous volume strongly increases from $0.02/0.008 \, \text{cm}^3 \, \text{g}^{-1}$ up to $0.148/0.219 \, \text{cm}^3 \, \text{g}^{-1}$ (significantly more for TA compared with DA). Concomitantly, the average pore size of the sorbent increases with metal sorption from 64 to 86 to 121–175. This order of magnitude corresponds to the predominance of mesopores. This expansion of porous properties with metal binding can be associated with the relative flexibility of the polymer network. The longer length of the amino chain and/or the lower sorption efficiency (see below) could explain the less marked effect on TA (compared with DA). Indeed, denser network of polymer-Pb(II) links may cause superior rigidity to the metal-bound structure.

The sorption and desorption profiles are characterized as Type II isotherm according to IUPAC classification [40], which corresponds to the presence of a large number of mesopores and/or macropores. In the case of DA, the hysteresis loop (associated with condensation effects) is hardly detectable contrary to TA (loop more marked, mainly in the range p/p_0 0.1–0.9); this is frequently associated with a wide distribution of pore sizes. In the case of metal loaded sorbents, both DA and TA show a significant loop (especially for $p/p_0 > 0.5$). The shape of the loop is close to Type H3; Singh [40] associates this profile with the formation of aggregates of plate-like particles approaching progressively slit-shaped pores. It is noteworthy that despite the similar synthesis routes and the very close chemical characteristics of the amine precursors, the textural properties of the two sorbents show marked differences (probably due to weaker stiffness in the case of TA).

3.2.3. Thermogravimetric analysis

The thermogravimetric analysis of the sorbents before and after Pb (II) sorption is summarized in Figure S7. In Figure S7a, the TGA shows several steps in the weight loss of the sorbents:

(a) 25–140 °C: the first step corresponds to the release of structural and superficial (adsorbed) water; the weight loss stands in the range of 6%.

(b) 140–470(TA)/485(DA): in this step, two waves can be observed associated with successive degradations of phenolic groups, amine groups, P-C bonds, phenylphonate [41], and depolymerization; the presence of phosphorus (as phosphonate) contributes to increased stability of the polymers; phosphorus is a well-known additive for improving the thermal stability of polymers [42]. This may explain that the additional weight loss represents between 42% (DA) and 46% (TA) (total weight loss 48 and 52%, respectively). It is noteworthy that the contribution of the first wave in the weight loss is more marked (and takes place in a larger range of temperature) for DA sorbent.

(c) Above 470–485 °C, the thermodegradation profile shows two other waves. This step corresponds to the pyrolysis of the chars formed during the previous degradation step. The weight loss reaches 92.3% at 780 °C for DA sorbent. It is noteworthy that, TA sorbent is more stable: the total weight loss does not exceed 82.5%, and a temperature of 900 °C is necessary for stabilizing the weight loss. Despite a similar amount of phosphorus in the two polymers (see below, Elemental analysis), TA is more stable than DA. In the degradation of the char, the second phase for DA sorbent shows stronger weight loss (about 27%).

The sorption of Pb(II) strongly improves the overall stability of the polymers. At 900 °C, the total weight loss does not exceed 49–53% (TA, and DA, respectively). Considering the sorption levels (see below), this strong increase in the residue cannot be simply explained by the presence of thermally stable compounds (bound metal). Indeed, the differences in the residues before and after metal sorption represents ≈40% (7.2/47.0%) for DA and ≈34% (17.6/51.2%) for TA. The binding of lead with reactive groups stabilizes the polymer. Pietrelli et al. [43] also reported the increase in the thermal stability of a polyacrylate derivative after copper sorption; although they also demonstrated that after metal desorption, the polymer conserved its good thermal stability.

The DTG curve (Figure S7b) highlights the similitudes and differences between the different materials. The peaks can be associated with the intermediary transitions in the TGA curves. The figure clearly illustrates both the strong impact of the amine precursor (chain length and the number of nitrogen) and the marked effect of Pb(II) sorption on degradation profiles. For example, the triamine precursor (TA) induces a new peak at 81.6 °C, a decrease in the intensity of the peak at 302.6 °C, the disappearance of the peak at 614.3 °C, and the decrease of the peak at 706.8 °C (compared with DA). On the other hand for DA, Pb(II) sorption shifts the peaks observed at 166.1 °C and 420.8 °C, the decrease in intensity of the peaks at 301.9 °C (associated with a little shift to lower temperature) and 614.3 °C, and the loss of the strong peak at 706.8 °C. In the case of TA, Pb(II) binding causes the disappearance of the peaks at 81.6 °C and 302/420.8 °C (which are replaced by a broad peak at 511.6 °C and a very sharp peak at 553.8 °C). In addition, the broad peak at 712.9 °C is shifted to 740.1 °C.

3.2.4. Elemental analysis

The elemental analysis of DA and TA sorbents confirms the effectiveness of the reaction between amine-bearing compounds and diphenyl phosphite/salicylaldehyde: the presence of both N and P elements demonstrates the formation of aminophosphonate (Table S3). The compositions of the sorbents are roughly the same for materials produced using the TiCl$_4$ and IL routes. The P content (weight percentage) in the sorbents is very close: 11.43 % and 10.29 % (i.e., 3.69 mmol P g^{-1}, and 3.32 mmol P g^{-1}, respectively) for DA and TA sorbents, respectively. As expected, N content in TA increases compared with DA. Consistently with the structure of the precursors (and sorbents) and suspected mechanisms, the N/P molar ratios are close to 0.8–0.86 and 1.34–1.39 for DA and TA sorbents (ranges for materials produced with TiCl$_4$ and IL routes), respectively: the increasing ratio is close to 1.65 between TA and DA. By simulation, it is possible suggesting the theoretical molecular formula of the sorbents (and their molecular weight): for diamine-precursor (DA; M.F.: $C_{40}H_{38}N_2O_8P_2$; MW: 736.21 g mol^{-1}) and triamine-precursor (TA; M.F.: $C_{42}H_{43}N_3O_8P_2$; MW: 779.75 g mol^{-1}). The theoretical number of mmoles per g of sorbents is of the same magnitude: 1.28 mmol for TA vs. 1.31 mmol DA. It is noteworthy that the fractions of C, H, N, and O roughly correspond to expected percentages (in weight) compared with the suggested structure, with the remarkable exception of the P element (where the found percentage exceeds the values deduced from the theoretical formula).

3.2.5. NMR analysis (^1H NMR, ^{13}C NMR, and ^{31}P NMR spectroscopies)

NMR analysis provides complementary information for confirming the structure of synthesized sorbents. In the ^1H NMR analysis (DMSO-d$_6$, 600 MHz), aromatic protons (Ar-H, 28H) are identified on both DA and TA sorbents, as confirmed by the appearance of a multiplet at $\delta = 6.843 \sim 7.65$ and $6.741 \sim 7.39$ ppm for DA-based and TA, respectively (Figure S8) [44]. Moreover, the proton on (P-C–H, 2H) chiral carbon forms a broad multiplet in the range $\delta = 4.671 \sim 4.85$ ppm for DA, while TA appears as a broad peak at $\delta = 4.20$ ppm [42].

In addition, the (N-CH$_2$, 4H) aliphatic methylene protons of DA appear as broad multiplet in the range $\delta = 3.395 \sim 3.556$ ppm, while the corresponding protons for TA (N-CH$_2$, 8H) are observed in the range $\delta = 3.06 \sim 3.14$ ppm. The (N–H, 2H) protons appear as a broad peak at $\delta =$

3.17 ~ 3.285 and 3.178 ~ 3.395 ppm for DA and TA, respectively [42].

Additionally, ^{13}C NMR analysis (DMSO-d$_6$, 150 MHz), both DA and TA sorbents show several carbon peaks consistent with each of the different chemical environments of the carbon atoms in the materials (Figure S9). The modification is identified by the disappearance of (C = O) peak for salicylaldehyde (identified at around δ = 193.04 ppm) and the appearance of the band of (P-CH) chiral carbon atom as a doublet at δ = 50.7 and 50.13 ppm. This doublet is characterized by a large coupling constant ($^1J_{PC}$ = 118.5, 130.5 Hz) due to carbon-phosphorous coupling for DA and TA respectively, while (Ar-OH) appears at δ = 157.85 and 157.86 ppm for DA and TA, respectively. In the case of Ar (8C), these carbons appear as multiple peaks ranging from 115.75 ~ 130.04 and 115.72 ~ 129.80 ppm for DA and TA, respectively. For (N-CH$_2$), the aliphatic chain appears at δ = 43.57 ppm for (2C) DA, and TA (4C) appears at δ = 43.85 and 44.85 ppm due to increase in chain length for TA.

The ^{31}P NMR analysis (DMSO-d$_6$, 243 MHz) appearing in Figure S10 confirms the existence of the phosphonate moiety associated with the P (O) signal at δ = 22.35 and 25.53 ppm for DA and TA, respectively [42]. The difference in ^{31}P NMR chemical shift signal between DA and TA sorbents by 3.18 ppm can be interpreted in terms of the difference in steric hindrance generated by surrounding bulky groups due to chain
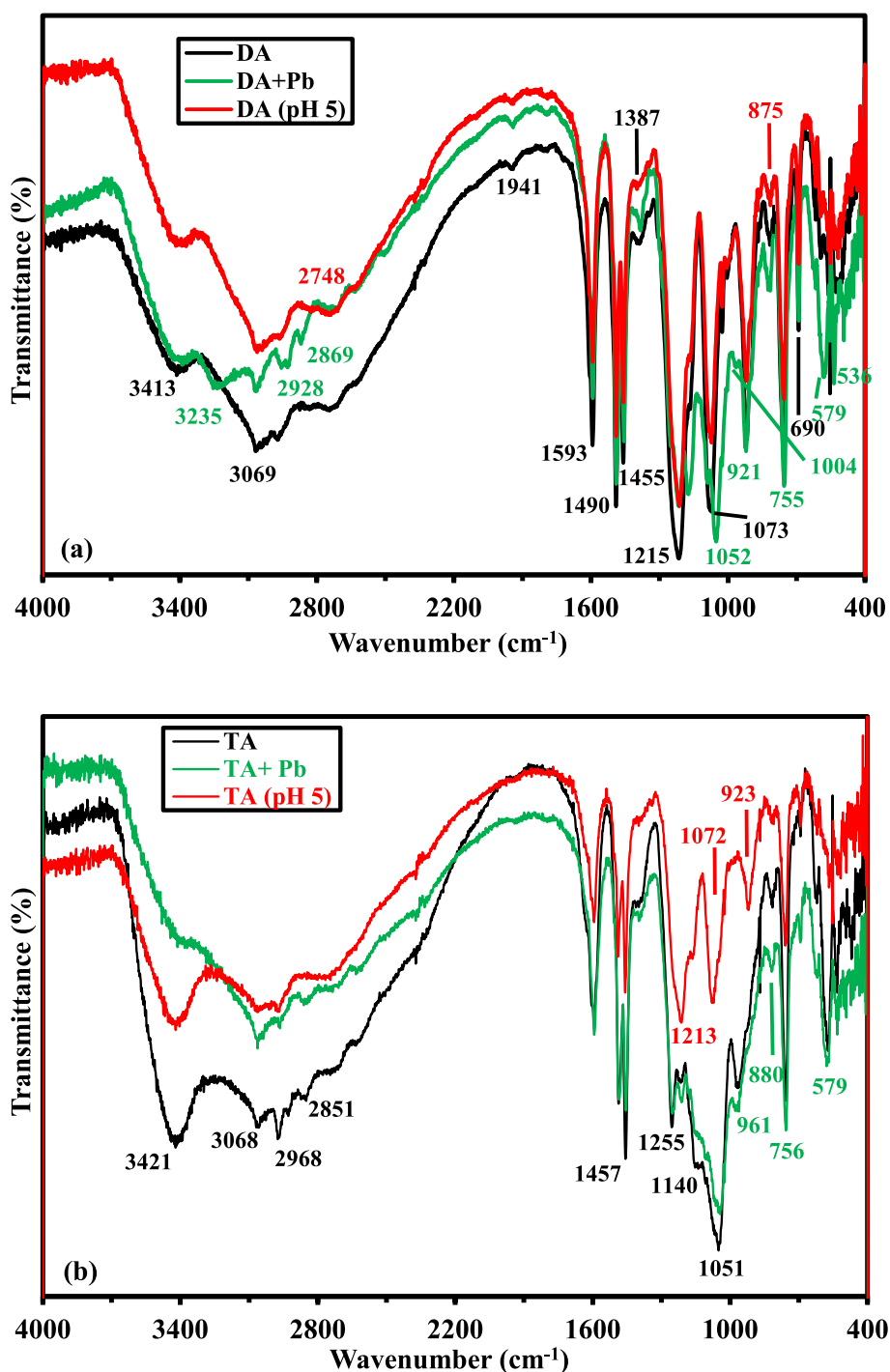

Fig. 1. FTIR spectra of DA and TA sorbents as-produced, after conditioning at pH 5, and after Pb(II) sorption at pH 5 (SD: 0.5 g L^{-1}; time: 12 h; T: 45 °C; C$_0$: 1.93 mmol Pb L^{-1}).

lengthening and/or -I effects of the third nitrogen on ^{31}P chemical shift. These two effects caused the shift of the phosphorus peak at the lower field in TA due to the minimized steric effect as well as the withdrawing (-I) effect of a midchain nitrogen atom when compared with DA.

3.2.6. Fourier transform infrared spectroscopy (FTIR

FTIR spectroscopy was used for the characterization of the functional groups on the sorbents and their interactions with Pb(II) (Fig. 1). The formation of DA- and TA-based α-aminophosphonates were confirmed by the appearance of the characteristic strong broad peaks at ≈1215 cm^{-1} for υ—P=O, 1073–1051 cm^{-1} for υP—O—C [45], 961–921 cm-1 for υ—P=O [46]. The intense signal at ≈756 cm^{-1} can be associated with the δN-H in aminophosphonate compounds [42]. The band at 3421–3413 cm^{-1} corresponds to the υNH overlapped with υOH. The band appearing around 3068 cm^{-1} (C= C—H), overlapped with both υNH and olefinic υCH. In addition, the aliphatic υCH appears at 2968–2928 cm-1, 2869–2851 cm^{-1}, and around 2748 cm^{-1}. The band at 1593 cm^{-1} is assigned to υC= C in aromatics. The bands at 1490 cm^{-1} and 1456 cm^{-1} are assigned to υC—N, and δC—H, respectively. The band at 690 cm^{-1} is attributed to υphenyl. With the increase in nitrogen content (in TA), the contributions of shoulders at 1631 cm^{-1} and 1606 cm^{-1} increase; they are assigned to amino groups (δNH scissoring) [47].

In Fig. 1, the spectra of pristine sorbents are compared with those of pH 5-conditioned sorbents and sorbents exposed to pb(II) solution (at the same pH), in order to differentiate the effects of environmental conditions (such as pH) from the proper interaction with Pb(II). In the case of DA, the most significant differences (not associated to pH effect) concern:

(a) the appearance of a new poorly resolved band at 3235 cm^{-1} (probably associated with the interaction of Pb(II) with amine groups).
(b) the shifts of υ—P=O and υP—O—C vibrations of phosphonate groups at around 1251 cm^{-1} and 1073 cm^{-1}. A small band also specifically appears at 1004 cm^{-1} after Pb(II) sorption, while the band at 553 cm^{-1} is replaced with twin bands at 579 and 536 cm^{-1}.

In the case of TA sorbent, the differences are less marked. A weak shoulder replaces the band at 3421 cm^{-1} (assigned to the overlapping of N—H and O—H stretching vibrations): amine groups are involved in metal binding. Surprisingly, contrary to the case of DA, the spectrum for TA conditioned at pH 5 significantly differs from the spectrum of the Pb (II)-loaded sorbent; notably in the 1260–950 cm^{-1}. On the opposite hand, the spectra of metal-loaded and pristine sorbents are relatively similar (with the remarkable exception of the N—H stretching vibration at 3421 cm^{-1}). Weak differences are observed on the profiles and the relative contributions of the bands at 1140 cm^{-1} and 1051 cm^{-1}; meaning that phosphonate groups are also involved in metal uptake.

The FTIR spectra of the sorbents after five cycles of sorption and desorption are reported in Figure S11. It is noteworthy that the spectra of pristine DA are very similar to the spectra of the recycled material and HCl-conditioned sorbent. The recycling of the sorbents shows a progressive decrease in sorption and desorption performances (see below). However, this decrease is relatively limited (about 10% at the fifth cycle). This is consistent with the remarkable stability of the FTIR spectrum. In the case of TA, the changes in the spectrum are more marked; it is remarkable that the changes for the recycled sorbent differ from the changes observed on the HCl-conditioned material. This means that the changes are not correlated with the alternating contacts of the sorbent with near-neutral and acid solutions. More specifically, the series of bands between 3068 and 2738 cm^{-1} are significantly reduced, while a new shoulder appears at 2414 cm^{-1}. The band at 1593 cm^{-1} is replaced by twin bands at 1593 and 1627 cm^{-1}; actually, the weak shoulder (on pristine sorbent) at 1640–1620 cm-1 forms a distinct band. However, the most significant changes appear in the range 1300–900

cm^{-1}, where are located the typical bands of phosphonate groups. This means that phosphonate moieties are significantly affected by the regeneration of the sorbent. The reason for a distinct effect of recycling steps compared with DA is not identified. The accumulation of lead ions (incomplete desorption) plays a more significant role in the case of TA. The length and number of amine groups in the linker influences the stability of sorbent structure; the triamine precursor is less favorable than the diamine one.

3.2.7. XPS analysis

X-ray photoelectron spectroscopy offers opportunities for characterizing the sorbents, but also their interactions with metal ions, as illustrated by Fig. 2. The XPS survey confirms the presence of C 1 s (at 285 eV), O 1 s (at 532 eV), N 1 s (at 402 eV) and P 2p (134–133 eV doublet, also including P 2 s signal, at 191 eV); this is consistent with the formation of an aminophosphonated polymer. The figure also displays the XPS survey curves for the sorbents exposed to Pb(II) solution: the binding of lead is confirmed by the appearance of two doublets at 144/ 139 eV (corresponding to Pb 4f$_{5/2}$ and Pb 4f$_{7/2}$, respectively) and 437/ 415 eV (assigned to Pb 4d$_{3/2}$ and Pb 4d$_{5/2}$, respectively). It is noteworthy that an additional doublet can be detected, mainly on TA sorbent exposed to Pb(II) solution at 465/459 eV (attributed to Ti 2p$_{1/2}$ and Ti 2p$_{3/2}$, respectively). These samples were produced with the TiCl$_4$/ acetonitrile synthesis routes; a residue of titanium remains adsorbed at the surface of the sorbents.

High-resolution XPS analysis allows identifying the chemical environment of target elements. Figures S12-S15 report the HR XPS spectra of C 1 s, O 1 s, N 1 s, and P 2p signals for DA and TA (before and after Pb (II) sorption). Table S4 summarizes the deconvolution of the peaks for the different signals with their BEs (binding energy, eV), AF (atomic percentage, %), and proposed assignments. The comparison of the deconvoluted signals for pristine sorbents show significant differences:

(a) C 1 s signal: little shifts for the 286.3 eV (to 285.9 eV) and 286.9 eV (to 286.6 eV) with inversion of their atomic fractions (≈25/15 %); this may be associated with the modification in the contribution of C-N and C-O-P functional groups. The strong contribution of C 1 s at 284.8 eV is related to the presence of phenyl groups.
(b) N 1 s: the change in the amine precursor strongly influences the deconvolution profile of this signal; the triamine precursor produces three deconvolution bands of approximately the same AF (29.3–39.6%), while in the case of DA, the major signal was identified close to 401.8 eV (corresponding to protonated amine assignment).
(c) P 2p: the spectra of pristine sorbents are characterized by 4 bands; two doublets (P 2p$_{3/2}$ and P 2p$_{1/2}$) associated with the predominant contribution of C-P (77.9% for DA and 88.6% for TA) and marginal contribution of O-P bonds (despite the greater number of O-P bonds).

It is noteworthy that the O 1 s signal is relatively stable when comparing DA and TA sorbents. Again, despite very similar precursors and the same synthesis route, the chemical characteristics are significantly influenced by the choice of diamine *vs.* triamine (as were the physical properties).

The analysis of the sorbents after Pb(II) sorption shows that C 1 s signal is hardly impacted: metal binding on vicinal elements (N for amine groups and O through phosphonate groups) does not significantly affect C 1 s contributions. The contribution of phosphonate to Pb(II) sorption is clearly identified through the changes observed in the signals:

(a) O 1 s: the relative contributions (AF values) (together with their BEs) are strongly affected by metal binding, and these changes are expressed differently for DA and TA. In the case of DA, the
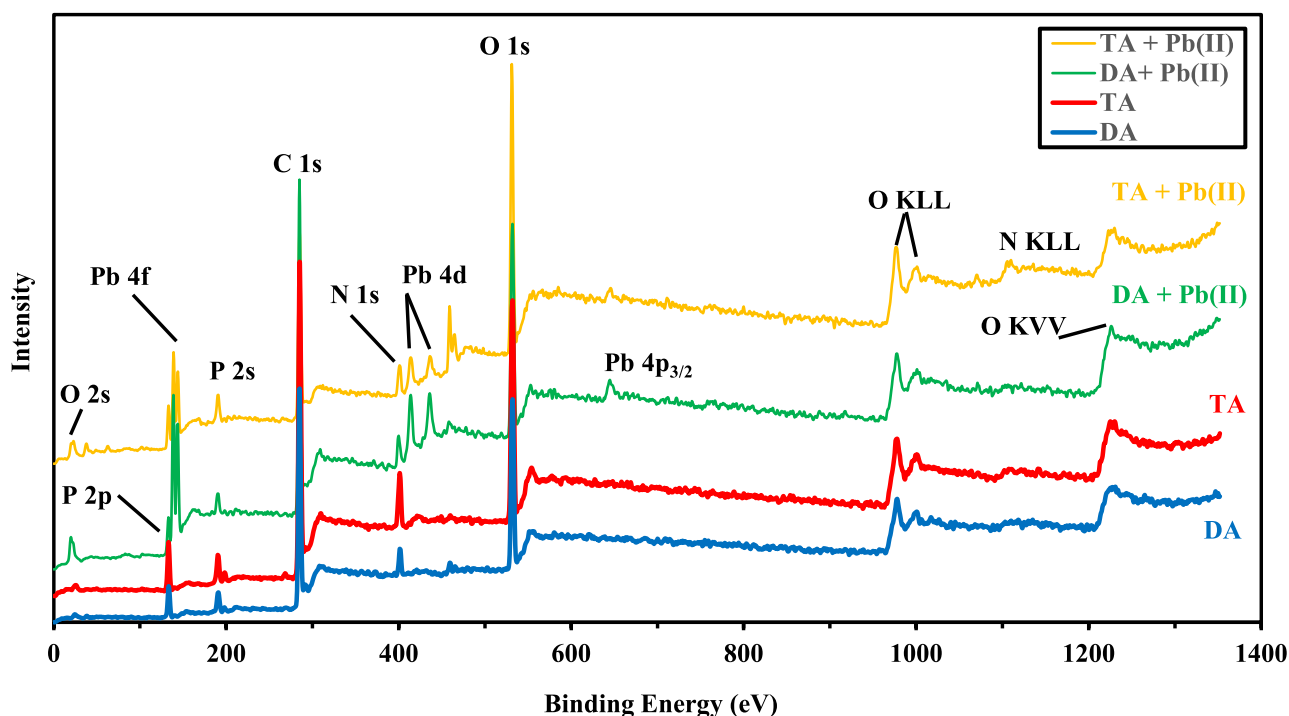
Fig. 2. XPS survey curve for DA and TA sorbents before and after Pb(II) sorption.

most significant changes appear at BEs: ≈531 eV (increase, assigned to O = P bond), ≈532 eV (increase, probably associated with P—O—Pb bond), and ≈533.1 eV (decrease in the contribution of P—O). However, the changes are much more significant for TA sorbent with strong decreases in the contributions O=P and P—OH signals (with shift from 531 eV to 530.5 eV, and ≈532.9 eV, respectively).

(b) P 2p: the contribution of O-P function disappears after Pb(II) sorption in the case of DA (only on doublet), while for TA, the contribution increases from 11.4% to 25.9% in the P 2p signal. The binding energies are poorly affected.

The amine groups are also involved in Pb(II) binding. Indeed, the AF of the different components are strongly modified. For DA sorbent, the contribution of amine groups strongly increases at the expense of a reduction of the signal associated with protonated amine groups (the signal is replaced by the contribution of the N-Pb bond). Similar trends are observed for TA: the contribution of protonated nitrogen is replaced with N-Pb bond (at ≈402 eV), C-N$^+$ contribution also decreases to the benefit of the N–H signal.

These observations confirm the contribution of O- and N- groups in the binding of Pb(II) (with impact on P 2p environment). The Pb 4f signal (Figure S16) shows the coexistence of two doublets (Pb 4f$_{7/2}$t and Pb 4f$_{5/2}$) that can probably be associated with O-Pb and N-Pb (with difficulty in formally assigning their relative contributions).

3.2.8. Determination of PZC

The determination of the PZC values brings important information on the surface charge of the sorbents and allows anticipating the eventual repulsion effects. Figure S17 compares the titration profiles using the pH-drift method for DA and TA sorbents. The PZC values are very close, around 3.77 for DA and 4.35 for TA. The incorporation of triamine (instead of diamine) gives a behavior little less acid compared with diamine precursor. The pK$_a$ of salicylaldehyde is reported close to 6.79, while the pKa values for amine-based compounds are frequently reported close to 9. On the other hand, diphenyl phosphite has a pKa value close to 9.0. The environment of phosphite strongly affects the acid-base

character: for example, Yu et al. 2013 [48] reported that the pK$_a$ of methyl diphosphate increases up to 18.4. The electron withdrawing forces of >P=O group reduces the electron density around the nitrogen atom of amino groups, which, in turn, decreases the pK$_a$ value of aminophosphonate [26]. The difference in the value of the PZC for the two sorbents can be directly associated with the negative inductive effect (−I) of the phenyl group: this group withdraws electron density through the single bond structure of the compound. It is worth noting that the presence of an extra basic amino group (>NH) in Triamine moiety increases the PZC from 3.77 to 4.35 which is attributed to the pKa's in the range 9.5 to 11.0, for the simple alkyl amines. This behavior affects the acid-base properties of aminophosphonates, and results in a lower pKa value [26,28]. Hägele et al. [49] investigated the acid-base properties of a series of aminophosphonate derivatives: the environment of the phosphonate group significantly affects the pK$_a$ values, which, in turn, controls the overall charge of the material. This may impact the response of the sorbent to pH effect (see below).

3.2.9. Binding mechanism

The characterization of the sorbents before and after Pb(II) sorption brings some insight into the mechanisms that could be involved in metal binding. Scheme 1 shows the presence of amine, phosphonate, and hydroxyl groups from the three constituents of the polymers (coming from diamine/triamine, diphenyl phosphite, and salicylaldehyde precursors). Assuming the coordination number for Pb(II) to be 6, it is possible suggesting that the metal can be bound through different modes of interaction, as reported in Scheme 2. The changes in the FTIR and XPS spectra demonstrated the contributions of amine and phosphonate groups. The complex can also be stabilized by binding on pending OH groups of salicylaldehyde moieties. These mechanisms involve:

(a) two ionic bonds, with the deprotonated oxygen atom of the hydroxyl group from salicylaldehyde moiety,

(b) two coordinating bonds, with nitrogen donors of amine groups, and.

(c) two coordinating bonds, with one oxygen donor of P = O groups from phosphonate groups.
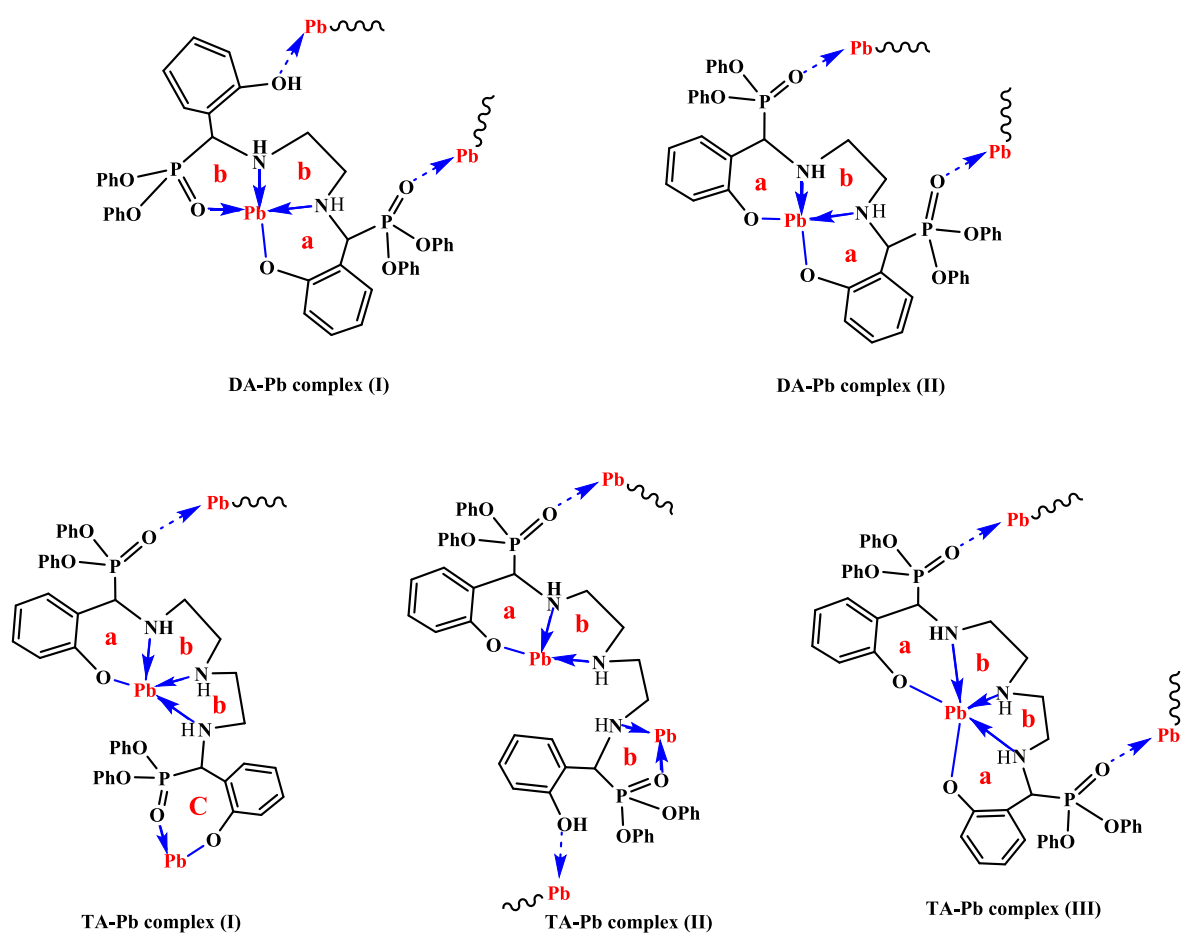
Scheme 2. Tentative complexation mechanism for Pb(II)-modes of interactions between reactive groups on both sorbents and Pb(II) ion complexes.

Thus, the contribution modes (a and b) form stable five- and six-membered chelating rings, while in other modes (C, in TA-Pb complex (I)) forms unstable and easily broken seven-membered rings. Moreover, the interaction of the metal ions between two chains, results in increasing the number of chelate rings (more chelation/binding opportunities).
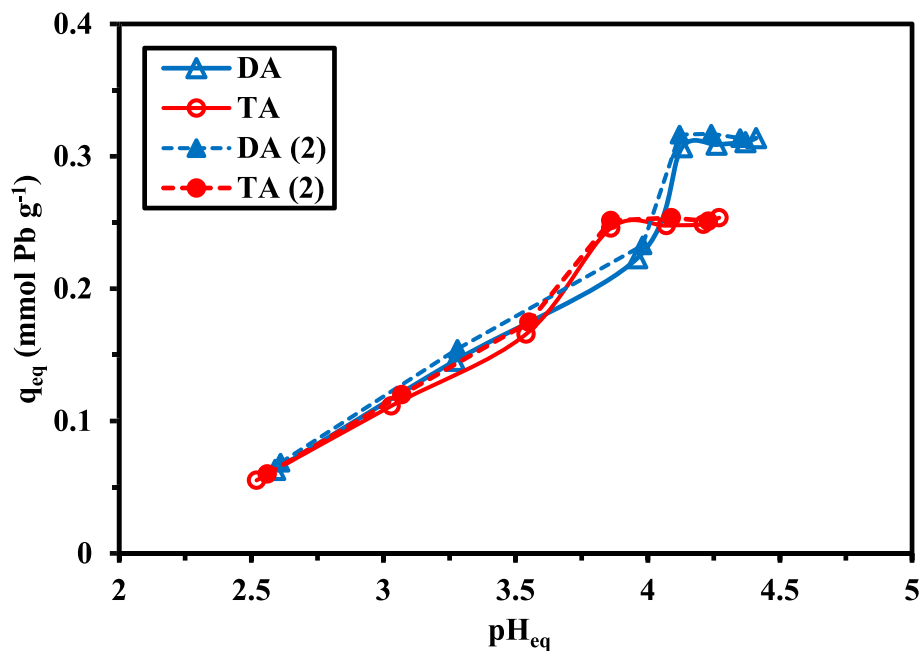

Fig. 3. Effect of pH on the sorption of Pb(II) using DA and TA sorbents (C_0: 0.244 mmol Pb L^{-1}; Sorbent dosage, SD: 0.5 g L^{-1}; T: 25 °C; v: 200 rpm; time: 720 min; reproducibility: duplicates).

3.3. Sorption studies

3.3.1. Effect of pH on Pb(II sorption

The pH of the solution is a critical parameter in optimizing metal sorption. This parameter may affect both the surface charge of the sorbent (in relation to PZC values) and the speciation of the metal (formation of specific complexes, hydroxides and colloids, and occurrence of precipitation). The protonation/deprotonation of reactive groups at the surface of the sorbent may induce attraction vs. repulsion effects. The formation of hydrolyzed species influences the ionic size of metal ions (and, consequently, their diffusion through the polymer network). Fig. 3 reports Pb(II) sorption capacity for DA and TA sorbents as a function of equilibrium pH. The initial pH value was varied between pH 2 and pH 8. The sorption capacity increases linearly with pH_{eq} between 2.5 and 4 for DA (from 0.063 to 0.22 mmol Pb g^{-1}); above pH 4, q_{eq} sharply increases to reach a maximum close to 0.31 mmol Pb g^{-1} (pH_0: 5). Above pH_{eq} 4.13, the sorption capacity stabilizes below 0.32 mmol Pb g^{-1}. Actually, for this last section of the curve, the initial pH of the solution is strongly shifted toward lower pH values (around 4–4.44) (Figure S18): the solution seems like buffered (despite not using buffer), and for the highest pH_0 values, the hydrolysis of lead takes place, including the appearance of precipitates (at pH higher than 6, Figure S19). Therefore, it is preferable to work at pH lower than 5.5 to avoid any interference from the precipitation mechanism. In the case of TA, the pH edge is globally similar; however, the sharp increase is reported at a lower pH value (i.e., pH_{eq} 3.86). The sorption capacity, under similar experimental conditions, does not exceed 0.26 mmol Pb g^{-1}: DA is a little more efficient than TA, despite the lower density of reactive groups (amino groups). Surprisingly, the sharp increase of sorption capacity with pH is shifted toward lower pH values, meaning in the opposite sense than the respective PZC values.

In acidic solutions, the protonation of reactive groups causes repulsion of metal cations, which are predominant as Pb^{2+} and $PbCl^+$ (Figure S19). With pH increase, this repulsion effect decreases, and the sorption of Pb(II) is gradually enhanced. At pH close to 4, the overall charge of sorbent surface is neutral while lead is present as Pb^{2+} (more 98%): the deprotonation of the reactive groups makes possible the binding of Pb^{2+} cations by complexation with amine groups and phosphonate moieties (with the contribution of deprotonated –OH groups from salicylaldehyde part of the polymer). At pH_0 higher than 4, the buffering effect shifts the equilibrium to pH $\approx$4.1–4.4, and the sorption capacity stabilizes. Increasing too much the pH_0 (above pH 6) causes the formation of hydrolyzed species and metal precipitation as hydroxide; the consumption of hydronium ions for metal precipitation contributes to the decrease of the pH.

The distribution ratio (D, L g^{-1}) is calculated from D = q_{eq}/C_{eq}. The log_{10}-plot of D vs. pH_{eq} is reported in Figure S20. The slope ranges between 0.52 and 0.59 (for TA and DA, respectively). This slope analysis is usually associated in ion-exchange processes with the stoichiometric ratio for proton exchange. In the current case, where both ion-exchange (-O(H) from salicylaldehyde moiety) and chelation (on amine groups and phosphonate) may be involved, the stoichiometric ratio refers to the number of protons released from reactive groups concomitantly to the binding of Pb(II) onto the sorbent: protons per Pb(II) cation bound to either DA and TA.

For both DA and TA sorbents, the highest sorption capacity is found for pH_0 $\approx$5 (with pH_{eq}: 3.4.13–3.86, respectively). This pH value is selected for further experiments. The speciation diagram shows that at this pH, lead is soluble even at the highest metal concentrations used to determine sorption isotherms (see below).

3.3.2. Uptake kinetics

The kinetic uptake may be controlled by different mechanisms associated with the stirring regime (resistance to bulk diffusion and film diffusion), the specific properties of the sorbent (specific surface area, porosity, and resistance to intraparticle diffusion), and/or to the proper reaction rate. Preliminary tests showed that a stirring speed of 150 rpm avoids particle settling and minimizes the effect of resistance to intraparticle diffusion. Textural analysis showed that the sorbents have a weak specific surface area (close to 6 m^2 g^{-1}). The pore size (determined by BJH calculation) ranges between 6.4 and 8.4 nm. This is typically within the size range of mesopores, as defined by IUPAC classification (i. e., 2–50 nm). This is also much larger than the hydrated radius size of lead ($Pb(H_2O)_6^{2+}$; i.e., 1.19 Å Shannon radius [50], meaning relatively free diffusion of metal ions into the mesoporous network of the polymer. It is noteworthy that after Pb(II) sorption, the textural properties are drastically increased; probably due to the swelling of the polymer structure and the expansion associated with lead intercalation. The small size of sorbent particles (about 34–36 μm) lets anticipate fast kinetics, confirmed by Fig. 4. The superposition of dupplicated series confirms the good reproducibility of sorption performances. The small size of the sorbent, their irregular surface, porosity make the initial section of the uptake kinetics very steep: within the first 30 min of contact, about 68% and 77% of total sorption take place (for DA and TA, respectively), and about 90% after 60 min of stirring. However, it is necessary to extend the contact time to 24 h to achieve the formal equilibrium corresponding to the supplementary recovery of 10% of total sorption. This means that slow sorption step takes part in the global sorption, probably associated with the resistance to intraparticle diffusion and to a less favorable concentration gradient between the solution and the core of the sorbent. Using small micro-particles is not sufficient to make negligible the effect of this step. Three conventional models have been used for simulating the kinetic profiles: the pseudo-first order rate equation, the pseudo-second order rate equation (PFORE and PSORE), and the Crank equation (for resistance to the intraparticle diffusion equation, RIDE) (Table S1a). Table S5 summarizes the parameters of these models together with the statistic evaluators of fits (i. e., R^2 and AIC). The values of statistical criteria for RIDE are significantly weaker than those of both PORE and PSORE: the RIDE fails to fit the region of the largest curvature of uptake kinetics (Figure S21). Herein, this equation is only used for evaluating the order of magnitude of the effective diffusion coefficient (i.e., D_e, m^2 min^{-1}): 1.73–1.77 × 10^{-12} m^2 min^{-1} and 2.86–2.68 × 10^{-12} m^2 min^{-1} for DA and TA, respectively. These values are about 4 orders of magnitude lower than the self-diffusivity of Pb(II) in water (i.e., 5.67 × 10^{-8} m^2 min^{-1}). This confirms that the resistance to intraparticle diffusion cannot be neglected. Fig. 4 superposed the fits with the PFORE and the PSORE to experimental profiles: the differences in the determination coefficients (i.e., R^2) and AIC values are not large enough to discriminate between the two models. For AIC, it is commonly accepted that differences are significant when $|\Delta$ AIC$|$ exceeds 2. Actually, the PFORE fits the initial section of the curve (up to 180 min) better but fails to reach the expected residual concentration (at 24 h). On the other hand, the PSORE approached well the equilibrium concentration, at the expense of a loss in the fits of the region of larger curvature. The comparison of calculated and experimental values for the sorption capacity at equilibrium ($q_{eq,exp}$ vs. $q_{eq,calc}$) is logically more favorable to the PSORE. Several researchers demonstrated the erroneous interpretation of model fits with reaction mechanisms (physical vs. chemical sorption) when inappropriate experimental conditions are selected [51,52]. One of the basic conditions, which is not fitted in most relevant studies, is the necessity to register a negligible variation of the solute concentration in the solution. This condition is rarely observed. Herein, the concentration variation is rather limited but probably insufficient to consider the concentration stable for making a correct interpretation. Therefore, the equations are only used for comparing the apparent rate coefficients (k_1 and k_2 parameters) for DA and TA. The sorption is kinetically more favorable onto TA with k_1 ($\approx$ 6.4 × 10^{-2} min^{-1}), and k_2 ($\approx$ 0.17 L $mmol^{-1}$ min^{-1}) values greater than those for DA ($\approx$ 4.7 × 10^{-2} min^{-1}, $\approx$ 8.1 × 10^{-2} L $mmol^{-1}$ min^{-1}, respectively). The initial section of the curve, which is usually controlled (within the first minutes of contact) by the resistance to film diffusion, is almost superposed for the two sorbents; herein, after the first 5 min of
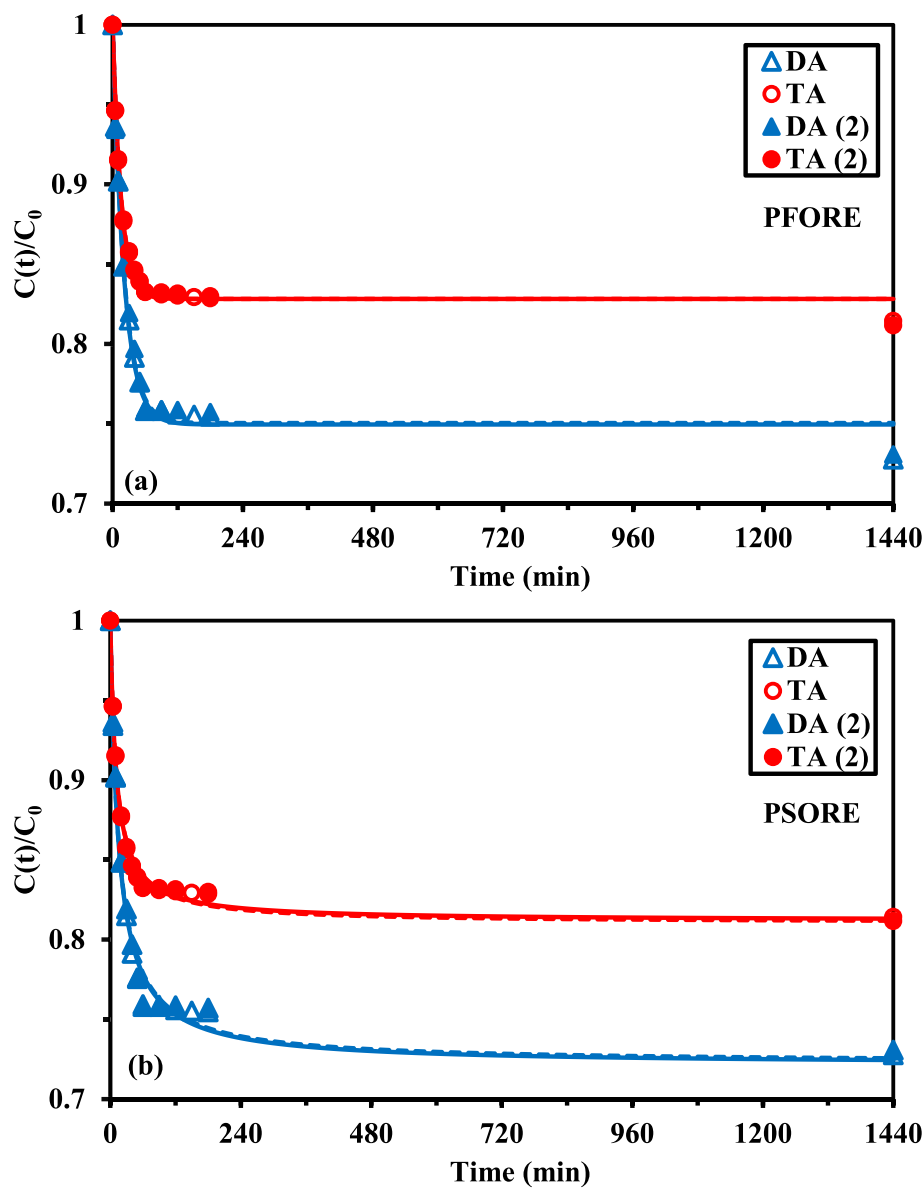
Fig. 4. Pb(II) uptake kinetics at pH_0 5 using DA and TA sorbents – Modeling with PFORE (a) and PSORE (b) (C_0: 1.45 mmol Pb L^{-1}; SD: 0.5 g L^{-1}; T: 25 °C; v: 200 rpm; reproducibility: duplicates).

contact Pb(II) is slightly faster sorbed onto TA (*vs.* DA). TA sorbent has little better textural properties than DA; this may contribute to speed up the sorption process. The larger number of reactive groups (triamine precursor) may also have an effect on the initial sorption (when the steric hindrance is not playing a significant effect). However, the sorption capacity at equilibrium is lower than for DA diamine precursor. These differences in transfer properties can be also correlated to the larger differences observed in the textural properties of the sorbents after metal binding (which are favorable to TA).

3.3.3. Sorption isotherms and thermodynamic parameters

The sorption isotherms plot the sorption capacities *vs.* equilibrium concentrations, representing the distribution of the solute, at equilibrium, under fixed conditions, between the liquid and solid phases. These isotherms bring important information on the maximum sorption capacity (at saturation of the sorbent), the affinity of the sorbent for target metal (correlated with the initial slope of the curve), and (to a certain extent) with the mechanisms possibly involved in metal binding (monolayer, multi-layer uptake, thermodynamics). Playing with the

temperature, it is also possible extracting the thermodynamic parameters. Fig. 5 compares Pb(II) sorption isotherms obtained at 25–55 °C for DA and TA sorbents. The superposition of duplicated series confirms the good repeatability in sorption experiments. The DA sorbent is characterized by a steep initial curve (high affinity) followed by a progressive increase in sorption capacity to reach a pseudo-plateau for residual concentration close to 1.5 mmol Pb L^{-1}. Although the global trend is similar for TA, its sorption isotherms are less favorable in the initial section (lower affinity) and reach a more marked plateau for a residual concentration close to 1.2 mmol Pb L^{-1}. It is noteworthy that for both DA and TA, the sorption of lead is enhanced when the temperature increases; however, this positive effect is apparently more marked for DA than for TA. The sorption is endothermic; this is generally associated with chemisorption processes. Whatever the temperature, Pb(II) sorption capacities for DA are superior to those of TA: maximum sorption capacity varies between 0.694 and 0.845 mmol Pb g^{-1} for DA as opposed to 0.494–0.594 mmol Pb g^{-1} for TA. Surprisingly, despite the higher number of reactive groups (meaning more amine groups) in TA, Pb(II) is more efficiently bound by DA. Frequently, the comparison of
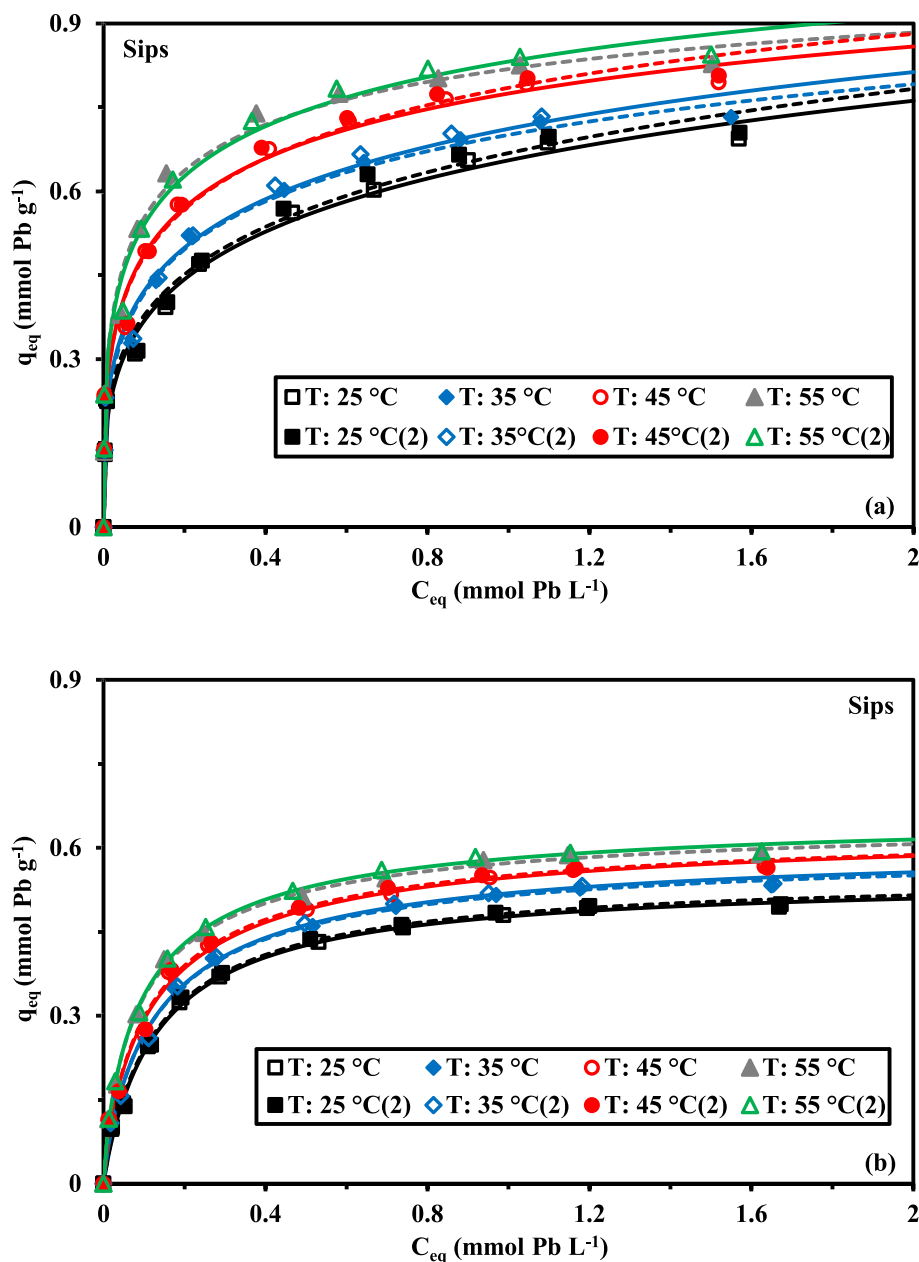
Fig. 5. Pb(II) sorption isotherms using DA (a) and TA (b) sorbents at pH$_0$ 5 – Modeling with Sips equation (C$_0$: 0–2 mmol Pb L^{-1}; SD: 0.5 g L^{-1}; time: 120 min; v: 200 rpm).

sorption performances refers to the principles of hard and soft acid base theory [53]. Here, the reactive groups are basically the same; the only change refers to the number of amine groups and the length of the amine precursor. This is probably this last parameter that may adversely impacts the sorption affinity of TA for Pb(II); the distance imposed by the longer chain does not accommodate finely to the coordination of the metal cation.

The sorption isotherms were fitted by Langmuir, Freundlich, Sips, Temkin and Dubinin-Raduskevich models (see Table S1b). The Langmuir equation supposes sorption as monolayer, without sorbent molecular interactions and homogeneous sorption energy. The LDS (Langmuir Dual Site equation) is based on the application of the Langmuir equation on heterogeneous sorbent bearing two types of sorption sites with different affinities for the solute. Freundlich empirical equation suggests the heterogeneous distribution of sorption energies possible interactions between sorbent molecules. This power-type model is not appropriate for fitting isotherms characterized by a saturation

plateau. The Sips equation combines Langmuir and Freundlich equations that can accommodate profiles with strong curvature and progressive saturation plateau [54]. The Temkin equation assumes that the sorption heat linearly decreases with the progressive saturation of the sorbent surface and that the sorption energies are uniformly distributed [55]. Recently, Chu [56] revisited the Temkin equation and pointed out the several mistakes commonly reported in the application of the equation, including dimension and units, and suggested an alternative complete isotherm. The Dubinin-Raduskevich equation assumes that the surface is not homogeneous or that the adsorption potential is not constant and that the sorption takes place into micropores [55]. The common formulation was recently debated by Hu and Zhang [57], who reported mistakes in the use of appropriate units for expressing concentrations (molar *vs.* mass) but also the wrong expression of the concentration term in the relevant equation. The concentration term should be C$_{eq}$/C$_s$ instead of C$_{eq}$ to make the term dimensionless and consistent with the original Temkin equation (C$_s$ being the solubility limit).

Tables S6 and S7 report the parameters (and statistical criteria) for DA and TA, respectively. In Fig. 5, the solid lines represent the Sips fitting of experimental curves, which is globally the most favorable (when taking into account all the series). However, apart the good mathematical fit, the Sips model drastically overestimates the maximum sorption capacity ($q_{m,S}$ *vs.* $q_{m,exp}$), especially for DA sorbent. Actually, the Langmuir models shows calculated values much closer to experimental data for the sorption at saturation of the monolayer. In the case of TA, the Langmuir equation finely simulates the profiles (Figure S22b), while Figure S22a fits the sorption isotherms for DA using the Langmuir Dual Site (LDS) equation:

$$q_{eq} = \frac{q_{m,L1} \times b_{L1} \times C_{eq}}{1 + b_{L1} \times C_{eq}} + \frac{q_{m,L2} \times b_{L2} \times C_{eq}}{1 + b_{L2} \times C_{eq}} \qquad (3)$$

where q_{mi}, (mmol Pb g^{-1}) and b_{Li} (L mmol^{-1}) are the sorption capacity at saturation of the monolayer and affinity coefficient for sites i = 1 and 2.

The LDS gives comparable statistical criteria for DA sorbent than the Sips equation. The contributions of Sites 1 and 2 are simulated in Figure S23. The Site 1 is characterized by a quasi-fixed maximum sorption capacity varying between 0.218 and 0.240 mmol Pb g^{-1} with an increasing affinity (from 392 to 1566 L mmol^{-1}). On the other hand, the Site 2 shows a growing contribution to metal binding at high metal concentration with a sorption capacity varying from 0.59 to 0.67 mmol Pb g^{-1} and an increasing affinity (from 2.65 to 9.84 L mmol^{-1}). The affinity of Site 2 for Pb(II) is about two orders of magnitude lower than Site 1.

The modeling with the Temkin equation gives relatively stable values for the b_T parameter ranging between 24.348 and 26.57 J kg mol^{-2} (regardless of sorbent and temperature). The energetic parameter E_T can be deduced from b_T values (i.e., $E_T = b_T/q_{m,exp}$): for both DA (from 37.0 to 31.2 kJ mol^{-1}) and TA (from 49.7 to 42.2 kJ mol^{-1}) the energetic parameter decreases with increasing temperature and remains higher than 20 kJ mol^{-1}, which is considered the limit for chemisorption processes. Conversely, the A_T coefficient strictly increases with temperature with both DA (from 721 to 2563 L mmol^{-1}) and TA (from 112 to 232 L mmol^{-1}). It is noteworthy that the values for TA are 6 to 10 times lower than the values found for DA sorbent. This confirms that the arrangement and the density of functional groups strongly influence the energetics of lead sorption. Herein, the conventional form of the Temkin was used after dimensional correction. The poor fits obtained with the Dubinin-Raduskevich equation make it difficult to determine the mean free energy of sorption (E_{DR}) accurately; the data should be considered only as an order of magnitude. The mean free energy decreases with increasing temperature (consistently with the enhanced favorability of metal sorption with temperature): from 8.94 to 12.0 kJ mol^{-1} and from 6.79 to 8.70 kJ mol^{-1} for TA.

The van'Hoff equation was used for analyzing the effect temperature on sorption isotherms and evaluating the thermodynamic parameters ($\Delta H°$ and $\Delta G°$, the changes in enthalpy and Gibbs free energy, respectively, kJ mol^{-1}; $\Delta S°$, the entropy change, J mol^{-1} K^{-1}) [58]:

$$\Delta G° = \Delta H° - T\Delta H° \qquad (4a)$$

$$\ln K_{eq}^0 = -\frac{\Delta H°}{R} \times \frac{1}{T} + \frac{\Delta S°}{R} \qquad (4b)$$

In the case of Langmuir equation (where b_L is expressed in L mol^{-1}):

$$K_{eq}^0 = b_L \times \frac{C_{sorbate}^0}{\gamma_{sorbate}} \qquad (4c)$$

where $C_{sorbate}^0$ is the unity standard concentration of the sorbate ($\approx$1 mol L^{-1}) and γ sorbate (dimensionless) is the activity coefficient of Pb(II) ($\approx$1, in dilute solutions).

Table S8 summarizes the thermodynamic parameters for Pb(II) sorption using DA and TA sorbents, at pH$_0$ 5 for T varying between 25 °C

and 55 °C); the plots of the van't Hoff equation are reported in Figure S24. The slopes are consistent for the duplicates; it is noteworthy that for DA sorbent a marked shift in the values of ln K$_0$ is observed between the two series. The enthalpy changes are positive for both DA and TA; meaning that lead sorption is endothermic. The enthalpy is higher for DA (i.e., 19.3–21.2 kJ mol^{-1}) than for TA (i.e., 11.5–12.0 kJ mol^{-1}). The entropy changes are also positive: 140.0–147.5 J mol^{-1} K^{-1} and 112.7–114.5 J mol^{-1} K^{-1} for DA and TA, respectively. These positive values mean that the entropy of the system increases with lead sorption: the randomness increases after metal sorption. This may be associated with the release of Cl$^-$, protons, and also the release of water from hydrated metal phases during the sorption process. In addition, the negative values of the changes in Gibbs free energy refer to the spontaneous sorption process. Logically, since sorption is endothermic, the spontaneity increases with temperature. The absolute value of T × $\Delta S°$ is systematically higher than $\Delta G°$ means that the sorption is rather controlled by entropic effect than by enthalpic criteria.

The dimensionless parameter, R_L, also called separation factor, is obtained by: $R_L = (1 + b·C_o)^{-1}$, where C_o is the Pb(II) initial concentration. The values of R_L provide information on the nature of the sorption process: when $R_L = 0$, the sorption is irreversible, while for $0 < R_L$ less than 1, the sorption is favorable. The case of $R_L = 1$ is associated with a linear sorption system (Henry equation), while the sorption is considered unfavorable when $R_L > 1$. At different initial concentrations and temperatures, the coefficient R_L was calculated for both DA and TA sorbents. The separation factor varies between 0.51 and 0.02 for DA-based sorbent and between 0.59 and 0.03 for TA-based sorbent, regardless of temperature. The sorption is favorable and favorability increases with metal concentration and temperature.

Table 1 compares the Pb(II) sorption properties of DA and TA sorbents with alternative sorbents reported in recent literature. DA sorbents show comparable sorption properties to the most efficient of these sorbents, considering the equilibrium and kinetic performances [8,10,44,59]. Lyu et al. [60] recently reported the outstanding sorption capacities obtained using modified red mud: the sorption capacity $q_{m,L}$ reached up to 2.84 mmol Pb g^{-1}. The combinations of different

Table 1
Comparison of sorption capacities for Pb(II) ions for various sorbents.

Sorbent	pH	Time	q$_{m,exp}$	q$_{m,L}$	b$_L$	Ref.
Sunflower stalk	5	240	0.724	0.694	10.8	[44]
Iodate-doped chitosan	6	240	–	0.107	65.1	[62]
Modified Amberlite XAD-4	7	240	0.132	0.136	7.04	[63]
L-cysteine/Magnetite NPs	6	30	–	0.0338	2955	[24]
Na-Y-zeolite/methyl methacrylate	4.5	90	0.834	–	–	[64]
Biosilica	4.8	360	0.531	0.584	12.3	[65]
Polyacrylonitrile/magnetite nanofibers	6	80	–	0.754	2.94	[59]
EDTA-functionalized bamboo activated carbon	5.3	360	0.579	0.596	106	[8]
Dipocolylamine/Amberlite XAD-16	5.6	60	0.55	0.581	2.86	[10]
L-lysine modified Montmorillonite	5.5	120	–	0.446	78.1	[21]
Functionalized sugarcane bagasse	5	120	0.967	1.16	3.31	[66]
Magnetic MnFe$_2$O$_4$@biochar	5	180	0.594	0.435	4.97	[13]
Hyper-crosslinked polystyrene	9	n.d.	0.917	1.18	6.22	[61]
Modified red mud	5	30	2.65	2.84	32.2	[60]
DA	5	120	0.694	0.714	9.89	*This work*
TA	5	120	0.494	0.540	7.66	*This work*

n.d.: not documented; T: $\approx$25 °C; Units – Time: mint; q$_m$: mmol Pb g^{-1}; b$_L$: L mmol^{-1}.

characterization methods showed the sorption of Pb(II) as carbonate species. Masoumi et al. [61] cited sorption capacities as high as 1.18 mmol Pb g^{-1} for hyper-crosslinked polystyrene; however, the sorption was performed in alkaline conditions; this is difficult comparing sorption performances under such different experimental conditions.

3.3.4. Sorption selectivity

In order to evaluate the potential of these materials for Pb(II) recovery, the sorption tests were extended to multicomponent equimolar solutions (C$_0$: 1 mmol L^{-1}) at pH$_0$ 5. In addition to Pb(II), alternative divalent metal cations were selected from base metals: Co(II), Ni(II), Zn (II), and Cd(II). The sorption capacities (q$_m$, mmol g^{-1}), distribution ratios (D, L g^{-1}), and selectivity coefficients (SC$_{metal/Co}$, Co(II) being used as the reference due to lower sorption capacities) are reported in Fig. 6 for both DA and TA sorbents. The sorbents have a marked preference for lead compared to alternative divalent cations: Pb(II) sorption capacities are twice to thrice those of other metals ions; the distribution ratio is 3 to 4 times higher for Pb(II). Basically, Co(II), Ni(II), Zn(II), and Cd(II) have roughly the same sorption performances. The preference of the sorbents for Pb(II) is also confirmed by the values of the selectivity coefficients (4.4–7.4) about 4 times the values of other heavy metals (0.9–1.4, with reference to Co(II)). It is noteworthy that DA is comparatively more efficient for Pb(II) sorption than TA; indeed, q$_{Pb}$(DA), D$_{Pb}$(DA), and SC$_{Pb/Co}$(DA) are systematically superior than the corresponding values for TA, while on the other side the parameters are more favorable for the sorption of other divalent cations for TA. This loss is selectivity for Pb(II) in the case of TA could be associated with the higher availability of the central amine group for the sorption of these metal ions. This effect may probably be explained by the difference in the ionic radius of Co(II), Ni(II), Zn(II), Cd(II) (in the range 0.69–0.95), much smaller than Pb(II) (i.e., 1.18). This size difference allows accommodating more to the accessibility and availability of reactive groups (which may be affected by steric hindrance and/or molecular

arrangements). These results are similar to those reported by Al-Saraj et al. [67] for Pb(II) sorption using free cells of *S. cerevisiae* and *S. cerevisiae* immobilized in sol–gel matrix composite. Phosphonate groups are well-known for being selective for Pb(II) ions [68].

Focusing on Pb(II), the sorption capacities reach 0.59 mmol Pb g^{-1} for DA and 0.44 mmol Pb g^{-1} for DA and TA, respectively. These values are close to the experimental maximum sorption capacities (i.e., 0.694 and 0.494 mmol Pb g^{-1}, respectively). This means that the presence of other metal ions (even in relative excess) does not inhibit Pb(II) sorption. The cumulative sorption capacities (on the five metals) reach 1.03 mmol g^{-1} and 1.00 mmol g^{-1} for DA and TA. These values exceed the maximum sorption capacities of Pb(II) (in mon-component solutions). This means that the other divalent cation metals can be bound to other reactive groups; this is even more marked for TA, where the cumulative sorption capacity is twice that reported for lead.

Annex A (see Supplementary Information) discusses the correlation between physicochemical characteristics of selected metal cations (Table S9) with their sorption properties (and selective specificities). The statistical analysis is biased by the grouped metals (Co, Ni, Zn, Cd) *vs.* Pb (Figure A1); however, this information provides interesting trends for assigning the selectivity and high sorption properties of DA (and to a lesser extent TA) for Pb(II) compared to alternative heavy metals ions. There is not a direct correlation between the HSAB ranking and the order of preference in metal sorption: Cd(II) is considered a soft acid while Co (II), Ni(II), Zn(II), and Pb(II) are borderline metals [53]. The causes for sorption preference for Pb(II) must be found elsewhere. The QSAR (qualitative structure–activity relationship) method allows discriminating the parameters the most representative for explaining the preference of the sorbents for lead. Four main parameters were pre-selected for their determination coefficients (Table A1): the atomic weight (AW, W symbol), the hydration enthalpy (-$\Delta G^0_{hydr.}$, D symbol), the acidity constant (pK$_{ae}$, K symbol) and more specifically the covalent index (X^2_m r, X symbol) (which shows the highest correlation). It is noteworthy that
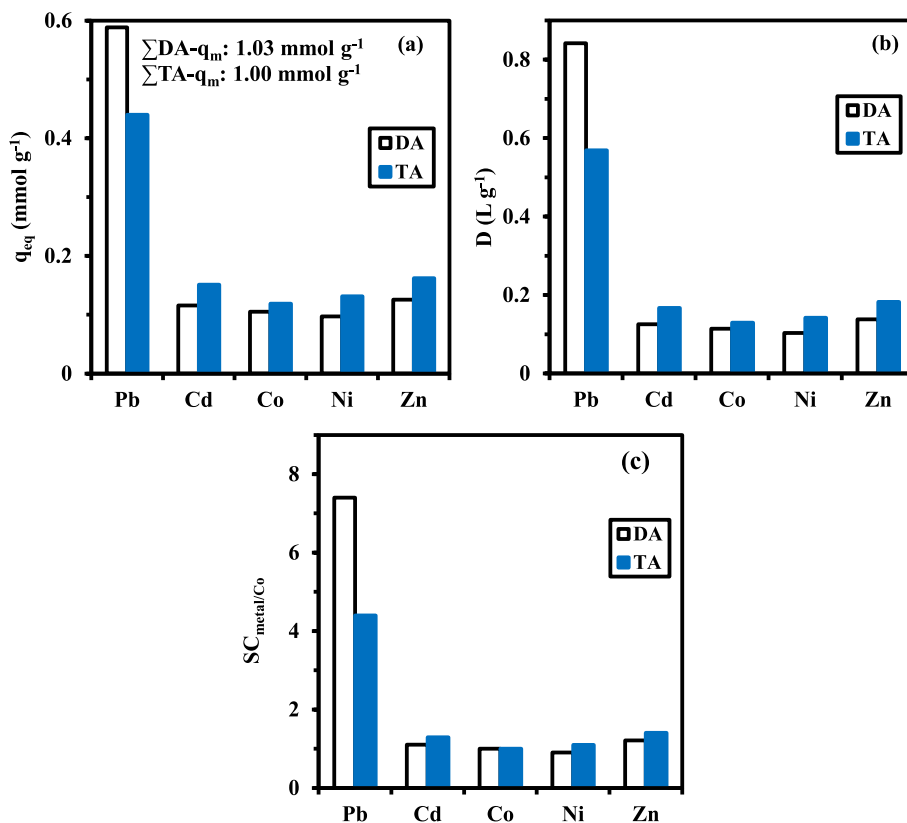

Fig. 6. Pb(II) sorption and separation from multicomponent equimolar solutions at pH$_0$ 5 using DA and TA sorbents: (a) sorption capacity (q$_{eq}$), (b) distribution ratio (D), and (c) SC$_{metal/Ni}$ (C$_0$: 1 mmol L^{-1}; SD: 0.5 g L^{-1}; T: 25 °C; time: 120 min; v: 200 rpm).

the covalent index is much more significant for describing the preference order than the ionic indices (such as the cation polarizing effect: Z^2 r, or the ionic potential: Z/r). This confirms the primary mode of interactions involving chelation of Pb(II) onto O-bearing and N-bearing groups rather than ion-exchange mechanism [69]. These conclusions have been confirmed in Table A2 by the analysis of the correlations used for these 4 parameters through AIC values. The most discriminating parameters in terms of sorption and selectivity are thus:

$$X_m^2 \, r > AW \approx - \Delta G_{hydr}^0 \approx pK_{ae}.$$

The sorption (and selectivity) parameters (P) have been successfully expressed as a function of these four descriptors based on the equation:

$$P = \alpha_0 + \alpha_W \times W + \alpha_X \times X + \alpha_D \times D + \alpha_K \times K \qquad (5)$$

Table A3 reports the relevant α values. Subject to the non-homogeneous distribution of the metals (groups metals *vs.* Pb), the high values of determination coefficients bring some useful trend for simulating the sorption performances. It would be useful to complete this approach with metal ions having "intermediary" characteristics.

3.3.5. Metal desorption and sorbent recycling.

Designing a new sorbent requires evaluating the capacity to valorize the metals and evaluate the capacity of sorbents to be recycled. Five successive cycles of sorption and desorption were performed under comparable conclusions. Since the sorption of Pb(II) is very sensitive to pH; an acidic solution was selected for testing metal desorption. More specifically, 0.2 M HCl solution was used for testing metal release and sorbent re-use; this level of concentration allows maintaining sufficient acidity for reversing metal sorption without being aggressive for the sorbent. Water rinsing between each step reduces the interferences in the sorption performances (washing of metal ions and softening of residual acidity). Table 2 summarizes the results collected along with the five cycles. For both DA and TA sorbents, the sorption efficiency progressively decreases: at the fifth cycle, the loss in sorption capacity reaches ≈ 12–14%. The desorption efficiency also progressively decreases from 98 to 96% at the first step to 86–84%. This may explain the progressive loss in sorption performance: some sorption sites remain occupied by stably-bound Pb(II). In addition, the FTIR analysis of the sorbent after the fifth desorption step showed that the spectra were modified in some regions associated with phosphonate groups (especially for TA, Figure S11). It would probably be helpful to investigate alternative desorption procedures (using a chelating agent or increasing acid concentration) to check if the stable fraction of bound-Pb is labile under other conditions.

3.3.6. Discussion of the effect of chain length of aliphatic amines on sorption properties

Chelating or coordinating ion-exchange resins are polymers with covalently bound functional groups (containing one or more donor atoms capable of forming complexes with metal ions). The functional groups the most frequently used are nitrogen-based (i.e., N as amine, azo, amide, or nitrile groups). Special attention was paid to the modification of chitosan by grafting polyamines ligands as ethylenediamine

(EDA) [70], diethylenetriamine (DETA) [71], and tetraethylenepentamine (TEPA) [72]. These modifications enhanced the sorption of mercury [73], uranyl [72], Th(IV) [74], and rare earths [70,71,75]. Grafting supplementary amino groups onto chitosan or PGMA backbone contributed not only to an increase in the sorption sites density but also to the enhancement of sorbent affinity by the appropriate steric distribution of reactive groups. Increasing the number of chelate rings increases the stability of complex formed with polyamine (it is noteworthy that this effect is only recorded for polyamine and not to functionalized amine groups) [71–74]. More specifically, Atia et al. [73] reported that the uptake capacities increase for Hg(II) with the increases of both the chain length and the number of reactive groups: TEPA > DETA > EDTA. For magnetic polymer composite functionalized with ethylenediamine and diethylenetriamine, Abd El-Magied et al. [74] correlated the enhancement of maximum sorption capacities for Th(IV) to the density of amine groups. The interaction between metal ions (i.e., U, Th) and amine groups on sorbent surface may be explained by chemisorption (involving valence forces such as sharing or exchange of electrons, complexation, coordination and chelation) [72,74]. However, DETA and TEPA exhibit different modes of coordination for interacting with metal ions: such as five-membered or eight (five membered) chelating rings with UO_2^{2+}; this mean that not only the number of amine groups may impact the sorption performance.

Herein, ethylenediamine and diethylenetriamine are used as amine precursors for the one-pot synthesis of aminophosphorylated sorbents. The sorption capacities of DA and TA for Pb(II) follow a reciprocal trend to that reported above for mono-functional sorbents (i.e., amine functionality only).

DA sorbent bears (a) two secondary amines are holding two lone pairs of electrons that can chelate metal ion, and (b) a salicylaldehyde moiety (bearing —OH group), and two phosphite moieties (bearing P=O groups), which also hold lone pairs of electrons that can also chelate to metal cations. In the case of TA sorbent, the central secondary amine (surrounded by alkyl groups) may be less reactive due to steric hindrance (due to these vicinal groups) and/or the distance with other reactive groups that inhibits their contribution to the complete coordination of Pb(II). The lower TA sorption efficiency (compared with DA) may be explained based on the –I effect of the mid N- in the triamine chain, which subsequently reduces the electron density of the two terminal nitrogen atoms (see above).

For TA-based sorbent, the unique possibility for metal ion (M^{n+}) binding consists of chelation by lone pair of electrons of salicylaldehyde —OH group and (P=O) group of phosphite. The contribution of the third N-atom in coordination leads to a more hindered structure with a polycyclic chelate structure with four rings (two five membered- and two six membered rings). For DA, it gives three rings (one five – and two six membered rings), i.e. less hindered and more favorable chelate structure (see Scheme 2: DA-Pb complex (II) and TA-Pb Complex (III)).

4. Conclusion

The one-pot synthesis of two aminophosphonate-based sorbents

Table 2

Sorbent recycling – Sorption capacity (q_{eq}, mmol g^{-1}) and desorption efficiency (DE, %) for 5 successive cycles of sorption and desorption using DA and TA sorbents.

Sorbent	DA				TA			
Cycle	q_{eq}		DE		q_{eq}		DE	
	#1	#2	#1	#2	#1	#2	#1	#2
1	0.607	0.625	97.0	98.0	0.491	0.507	95.9	97.1
2	0.586	0.607	94.1	95.2	0.468	0.488	93.3	94.8
3	0.561	0.585	91.5	92.9	0.455	0.470	91.7	92.0
4	0.544	0.569	88.7	90.4	0.441	0.459	88.1	89.7
5	0.526	0.547	86.3	88.9	0.421	0.442	84.4	86.1
Loss 5th/1st	−13.4%	−12.5%	−11.0%	−9.3%	−14.3%	−12.8%	−12.0%	−11.4%

Sorption: C_0: 1.44 mmol Pb L^{-1}; SD: 0.5 g L^{-1}; pH$_0$ 5; T: 25 °C; Time: 2 h; desorption: 0.2 M HCl eluent solution; SD: 2 g L^{-1}; T: 25 °C; time: 30 min).

(using alternatively ionic liquid or TiCl$_4$/acetonitrile as the catalytic system) by reaction of salicylaldehyde, diphenyl phosphite and polyamine precursors allows producing efficient sorbents for Pb(II) recovery from aqueous solutions. NMR analyses together with FTIR and XPS analyses (including titration and elemental analysis) confirm the structure of the micron-size sorbents. The simple enlargement of the amine chain (increased number of amine groups) significantly changes both the textural and the sorption properties of the materials. Surprisingly, introducing a greater number of amine groups (diethylenetriamine for TA vs. ethylenediamine for DA) reduces the sorption performance and the selectivity of the sorbents for Pb(II). Several reasons may cause this effect such as the arrangement of the reactive groups (–OH from salicylaldehyde, P=O groups from phosphonate moieties, and amine groups from amine linker) reveals more favorable (due to chain and link lengths and/or electronic –I effect of central nitrogen in TA as well as the number of congested polycyclic chelate rings). FTIR and XPS analyses confirm the contribution of these reactive groups. The sorption mainly involves chelation mechanisms (vs. minor ionic interactions).

Optimum sorption of lead occurs at pH close to 5 (with significant pH decrease during metal sorption). The uptake is fast (reaching a quasi-equilibrium within 60–120 min), and the kinetic profiles can be fitted by both pseudo-first order and pseudo-second order rate equations (almost equally). Despite the micron-size of the sorbents, the contribution of resistance to intraparticle diffusion cannot be neglected (especially for the last phase of the sorption process). The sorption isotherms can be modeled using the Sips equation; however, for TA sorption, the Langmuir equation is also giving a good fit of experimental profile. It is noteworthy that for DA sorbent, the Langmuir Dual Site model is much better than the Langmuir equation. This is another evidence of the marked differences between DA and TA sorbents: the simple introduction of the central amine function significantly influences the sorption behavior.

DA sorbent is highly selective to Pb(II) compared with other divalent metal cations, such as Co(II), Ni(II), Zn(II), and Cd(II). This sorbent is more selective than TA. The sorption and selectivity performances in multi-component equimolar solutions can be correlated to several parameters, including atomic weight, acid characteristics, energy of hydration, and more specifically, the covalent index.

The sorbents can be regenerated using 0.2 M HCl solutions. However, after fives cycles both the sorption and desorption performances lose about 12–14% (compared with initial performances).

The prepared DA and TA could be regarded as potential adsorbents for efficient removal of Pb(II) from aqueous media, and could be further utilized for environmental waste management.

Declaration of Competing Interest

The authors declare that they have no known competing financial interests or personal relationships that could have appeared to influence the work reported in this paper.

Acknowledgements

Appendix A. Supplementary data

Supplementary data to this article can be found online at https://doi.org/10.1016/j.cej.2022.136300.

References

[1] Z. Lin, Y. Hu, Y. Yuan, B. Hu, B. Wang, Comparative analysis of kinetics and mechanisms for Pb(II) sorption onto three kinds of microplastics, Ecotoxicol. Environ. Saf. 208 (2021), 111451.

[2] X. Yang, Y. Wan, Y. Zheng, F. He, Z. Yu, J. Huang, H. Wang, Y.S. Ok, Y. Jiang, B. Gao, Surface functional groups of carbon-based adsorbents and their roles in the removal of heavy metals from aqueous solutions: a critical review, Chem. Eng. J. 366 (2019) 608–621.

[3] L. Joseph, B.-M. Jun, J.R.V. Flora, C.M. Park, Y. Yoon, Removal of heavy metals from water sources in the developing world using low-cost materials: A review, Chemosphere 229 (2019) 142–159.

[4] P. Kumar, A. Pournara, K.-H. Kim, V. Bansal, S. Rapti, M.J. Manos, Metal-organic frameworks: Challenges and opportunities for ion-exchange/sorption applications, Prog. Mater. Sci. 86 (2017) 25–74.

[5] F. Parsadoust, M. Shirvani, H. Shariatmadari, M. Dinari, Effects of GLDA, MGDA, and EDTA chelating ligands on Pb sorption by montmorillonite, Geoderma 366 (1) (2020), 114229.

[6] D. Luo, R. Geng, W. Wang, Z. Ding, S. Qiang, J. Liang, P. Li, Y. Zhang, Q. Fan, Trichoderma viride involvement in the sorption of Pb(II) on muscovite, biotite and phlogopite: batch and spectroscopic studies, J. Hazard. Mater. 401 (2021) 123249.

[7] Z. Zhang, K. Chen, Q. Zhao, M. Huang, X. Ouyang, Comparative adsorption of heavy metal ions in wastewater on monolayer molybdenum disulfide, Green Energy Environ. 6 (5) (2021) 751–758.

[8] D. Lv, Y. Liu, J. Zhou, K. Yang, Z. Lou, S.A. Baig, X. Xu, Application of EDTA-functionalized bamboo activated carbon (BAC) for Pb(II) and Cu(II) removal from aqueous solutions, Appl. Surf. Sci. 428 (2018) 648–658.

[9] E.-S.-M. El-Sayed, D. Yuan, Waste to MOFs: sustainable linker, metal, and solvent sources for value-added MOF synthesis and applications, Green Chem. 22 (13) (2020) 4082–4104.

[10] A. Chauhan, A. Islam, H. Javed, S. Kumar, Facile fabrication of Amberlite XAD-16 with dipicolylamine for remediation of industrial wastewater containing lead and copper: Isotherm, kinetics, thermodynamics and selectivity studies, Microchem. J. 146 (2019) 606–613.

[11] F.J. Alguacil, The removal of toxic metals from liquid effluents by ion exchange resins. Part IX: Lead(II)/H+/Amberlite IR-120, Revista de Metalurgia 55 (1) (2019) 138.

[12] A. Agrawal, K.K. Sahu, Separation and recovery of lead from a mixture of some heavy metals using Amberlite IRC 718 chelating resin, J. Hazard. Mater. 133 (1) (2006) 299–303.

[13] F. Guzel, C. Yilmaz, Synthesis, characterization, and lead (II) sorption performance of a new magnetic separable composite: MnFe$_2$O$_4$@wild plants-derived biochar, J. Environ. Chem. Eng. 9 (1) (2021) 104567.

[14] B.V. Joshi, B. Vipin, J. Ramkumar, R.K. Amit, Impact of policy instruments on lead-acid battery recycling: A system dynamics approach, Resour. Conserv. Recycl. 169 (2021) 105528.

[15] J. Li, C. Duan, L. Yuan, Z. Liu, H. Zhu, J. Ren, K. Yan, Recycling spent lead-acid batteries into lead halide for resource purification and multifunctional perovskite diodes, Environ. Sci. Technol. 55 (12) (2021) 8309–8317.

[16] X. Tian, H. Xiao, Y. Liu, W. Ding, Design and simulation of a secondary resource recycling system: A case study of lead-acid batteries, Waste Manage. (Oxford) 126 (2021) 78–88.

[17] S.D. Alexandratos, X.P. Zhu, M. Florent, R. Sellin, Polymer-supported bifunctional amidoximes for the sorption of uranium from seawater, Ind. Eng. Chem. Res. 55 (15) (2016) 4208–4216.

[18] J. Muller, B. Prelot, J. Zajac, S. Monge, Synthesis and study of sorption properties of polyvinyl alcohol (PVA)-based hybrid materials, React. Funct. Polym. 144 (2019), 104364.

[19] M.M. Rashad, I.E. El-Sayed, A.A. Galhoum, M.M. Abdeen, H.I. Mira, E.A. Elshehy, S. Zhang, X. Lu, J. Xin, E. Guibal, Synthesis of α-aminophosphonate based sorbents – Influence of inserted groups (carboxylic vs. amine) on uranyl sorption, Chem. Eng. J. 421 (2021), 127830.

[20] Y. Zhou, Y. Gao, H. Wang, M. Xia, Q. Yue, Z. Xue, J. Zhu, J. Yu, W. Yin, Versatile 3D reduced graphene oxide/poly(amino-phosphonic acid) aerogel derived from waste acrylic fibers as an efficient adsorbent for water purification, Sci. Total Environ. 776 (2021) 145973.

[21] S. Zhu, M. Xia, Y. Chu, M.A. Khan, W. Lei, F. Wang, T. Muhmood, A. Wang, Adsorption and desorption of Pb(II) on l-lysine modified montmorillonite and the simulation of interlayer structure, Appl. Clay Sci. 169 (2019) 40–47.

[22] S.D. Alexandratos, S. Natesan, Ion-selective polymer-supported reagents: the principle of bifunctionality, Eur. Polym. J. 35 (3) (1999) 431–436.

[23] S.D. Alexandratos, S.D. Smith, Intraligand cooperation in metal-ion binding by immobilized ligands: The effect of bifunctionality, J. Appl. Polym. Sci. 91 (1) (2004) 463–468.

[24] Y. Bagbi, A. Sarswat, D. Mohan, A. Pandey, P.R. Solanki, Lead and chromium adsorption from water using L-cysteine functionalized magnetite (Fe$_3$O$_4$) nanoparticles, Sci. Rep. 7 (1) (2017) 7672.

[25] A.A. Galhoum, E.A. Elshehy, D.A. Tolan, A.M. El-Nahas, T. Taketsugu, K. Nishikiori, T. Akashi, A.S. Morshedy, E. Guibal, Synthesis of polyaminophosphonic acid-functionalized poly(glycidyl methacrylate) for the efficient sorption of La(III) and Y(III), Chem. Eng. J. 375 (2019) 121932–121948.

[26] V.P. Kukhar, V. Romanenko, Chemistry of aminophosphonic acids and phosphonopeptides, Wiley-VCH verlag GmbH & C, KGaA, Weinheim, Germany, 2010.

[27] A.A. Galhoum, W.H. Eisa, I.-E.-T. El-Sayed, A.A. Tolba, Z.M. Shalaby, S. I. Mohamady, S.S. Muhammad, S.S. Hussien, T. Akashi, E. Guibal, A new route for

manufacturing poly(aminophosphonic)-functionalized poly(glycidyl methacrylate)-magnetic nanocomposite- Application to uranium sorption from ore leachate, Environ. Pollut. 264 (2020), 114797.

[28] E.A. Imam, I. El-Tantawy El-Sayed, M.G. Mahfouz, A.A. Tolba, T. Akashi, A. A. Galhoum, E. Guibal, Synthesis of α-aminophosphonate functionalized chitosan sorbents: Effect of methyl vs phenyl group on uranium sorption, Chem. Eng. J. 352 (2018) 1022–1034.

[29] A.S. Morshedy, A.A. Galhoum, A. Aleem, H. Abdel Aleem, M.T. Shehab El-din, D. M. Okaba, M.S. Mostafa, H.I. Mira, Z. Yang, I.-E.-T. El-Sayed, Functionalized aminophosphonate chitosan-magnetic nanocomposites for Cd(II) removal from aqueous solutions: performance and mechanisms of sorption, Appl. Surf. Sci. 561 (2021), 150069.

[30] M.E. Mahmoud, S.E. Adel, I.E.T. El-Sayed, Development of titanium oxide-bound-α-aminophosphonate nanocomposite for adsorptive removal of lead and copper from aqueous solution, Water Resour. Ind. 23 (2020), 100126.

[31] B. Shah, U. Chudasama, Kinetics, thermodynamics and metal separation studies of transition (Co^{2+}, Ni^{2+}, Cu^{2+}, Zn^{2+}) and heavy metal ions (Cd^{2+}, Hg^{2+}, Pb^{2+}) using novel hybrid ion exchanger: zirconium amino tris methylene phosphonic acid, Sep. Sci. Technol. 54 (2019) 1560–1572.

[32] S. Saoiabi, K. Achelhi, S. Masse, A. Saoiabi, A. Laghzizil, T. Coradin, Organo-apatites for lead removal from aqueous solutions: A comparison between carboxylic acid and aminophosphonate surface modification, Colloids Surf. A: Physicochem. Eng. Asp. 419 (2013) 180–185.

[33] R. Kiefer, W.H. Höll, Sorption of heavy metals onto selective ion-exchange resins with aminophosphonate functional groups, Ind. Eng. Chem. Res. 40 (2001) 4570–4576.

[34] R. Kiefer, A.I. Kalinitchev, W.H. Höll, Column performance of ion exchange resins with aminophosphonate functional groups for elimination of heavy metals, React. Funct. Polym. 67 (2007) 1421–1432.

[35] A. Thompson, D. Attwood, E. Gullikson, M. Howells, K.-J. Kim, J. Kirz, J. Kortright, I. Lindau, Y. Liu, P. Pianetta, A. Robinson, J. Scofield, J. Underwood, G. Williams, H. Winick, X-ray data booklet, lawrence berkeley national laboratory, university of California, Berkeley, CA, USA, (2009).

[36] Y. Tian, L. Liu, F. Ma, X. Zhu, H. Dong, C. Zhang, F. Zhao, Synthesis of phosphorylated hyper-cross-linked polymers and their efficient uranium adsorption in water, J. Hazard. Mater. 419 (2021) 126538.

[37] M. Wang, C. Shi, J. Zhang, N. Wu, C. Ying, Influence of $PbCl_2$ content in PbI_2 solution of DMF on the absorption, crystal phase, morphology of lead halide thin films and photovoltaic performance in planar perovskite solar cells, J. Solid State Chem. 231 (2015) 20–24.

[38] A.M. Yousif, O.F. Zaid, I.A. Ibrahim, Fast and selective adsorption of As(V) on prepared modified cellulose containing Cu(II) moieties, Arabian J. Chem. 9 (5) (2016) 607–615.

[39] N.F. Attia, S.M. Lee, H.J. Kim, K.E. Geckeler, Nanoporous polypyrrole: preparation and hydrogen storage properties, Int. J. Energy Res. 38 (2014) 466–476.

[40] K.S.W. Sing, Reporting physisorption data for gas/solid systems with special reference to the determination of surface area and porosity (recommendations 1984), Pure Appl. Chem. 57 (4) (1985) 603–619.

[41] A. Popa, R. Ene, D. Visinescu, E.S. Dragan, G. Ilia, S. Iliescu, V. Parvulescu, Transitional metals immobilized by coordination on aminophosphonate functionalized copolymers and their catalytic properties, J. Mol. Catal. A Chem. 408 (2015) 262–270.

[42] J.J. Qiu, Q. Xue, Y.Y. Liu, M. Pan, C.M. Liu, A new polymer containing α-aminophosphonate unit used as reactive, halogen-free flame retardant for epoxy resins, Phosphorus Sulfur Silicon Relat. Elem. 189 (3) (2014) 361–373.

[43] L. Pietrelli, M. Palombo, V. Taresco, F. Crisante, I. Francolini, A. Piozzi, Copper (II) adsorption capacity of a novel hydroxytyrosol-based polyacrylate, Polym. Bull. 74 (4) (2017) 1175–1191.

[44] M. Jalali, F. Aboulghazi, Sunflower stalk, an agricultural waste, as an adsorbent for the removal of lead and cadmium from aqueous solutions, J. Mater. Cycles Waste Manage. 15 (4) (2013) 548–555.

[45] S. Rasal, S. Jain, N.G. Shimpi, Reusable zinc oxide nanoflowers for the synthesis of aminophosphonates under solvent-free ultrasonication, Synth. Commun. 48 (18) (2018) 2420–2434.

[46] M.F. Cheira, Synthesis of aminophosphonate-functionalised ZnO/polystyrene-butadiene nanocomposite and its characteristics for uranium adsorption from phosphoric acid, Int. J. Environ. Anal. Chem. 101 (12) (2020) 1710–1734.

[47] D. Lin-Vien, N.B. Colthup, W.G. Fateley, J.G. Grasselli, Chapter 10: compounds containing –NH₂, –NHR, and –NR₂ groups, the handbook of infrared and Raman characteristic frequencies of organic molecules, Academic Press, San Diego, 1991.

[48] B. Yu, H. Zhang, Y. Zhao, S. Chen, J. Xu, L. Hao, Z. Liu, DBU-based ionic-liquid-catalyzed carbonylation of o-phenylenediamines with CO_2 to 2-benzimidazolones under solvent-free conditions, ACS Catal. 3 (9) (2013) 2076–2082.

[49] G. Hägele, Z. Szakács, J. Ollig, S. Hermens, C. Pfaff, NMR-controlled titrations: characterizing aminophosphonates and related structures, Heteroat. Chem 11 (7) (2000) 562–582.

[50] I. Persson, Hydrated metal ions in aqueous solution: How regular are their structures? Pure Appl. Chem. 82 (10) (2010) 1901–1917.

[51] M.A. Hubbe, S. Azizian, S. Douven, Implications of apparent pseudo-second-order adsorption kinetics onto cellulosic materials: A review, BioRes. 14 (3) (2019) 7582–7626.

[52] J.-P. Simonin, On the comparison of pseudo-first order and pseudo-second order rate laws in the modeling of adsorption kinetics, Chem. Eng. J. 300 (2016) 254–263.

[53] R.G. Pearson, acids and bases, Sci. (New York) 151 (3707) (1966) 172–177.

[54] C. Tien, adsorption Calculations and Modeling, Butterworth-Heinemann, Newton, MA, 1994.

[55] K.Y. Foo, B.H. Hameed, Insights into the modeling of adsorption isotherm systems, Chem. Eng. J. 156 (1) (2010) 2–10.

[56] K.H. Chu, Revisiting the Temkin isotherm: Dimensional inconsistency and approximate forms, Ind. Eng. Chem. Res. 60 (35) (2021) 13140–13147.

[57] Q. Hu, Z. Zhang, Application of Dubinin-Radushkevich isotherm model at the solid/solution interface: A theoretical analysis, J. Mol. Liq. 277 (2019) 646–648.

[58] H.N. Tran, E.C. Lima, R.-S. Juang, J.-C. Bollinger, H.-P. Chao, Thermodynamic parameters of liquid–phase adsorption process calculated from different equilibrium constants related to adsorption isotherms: A comparison study, J. Environ. Chem. Eng. 9 (6) (2021) 106674.

[59] H. Malik, U.A. Qureshi, M. Muqeet, R.B. Mahar, F. Ahmed, Z. Khatri, Removal of lead from aqueous solution using polyacrylonitrile/magnetite nanofibers, Environ. Sci. Pollut. Res 25 (4) (2018) 3557–3564.

[60] F. Lyu, S. Niu, L. Wang, R. Liu, W. Sun, D. He, Efficient removal of Pb(II) ions from aqueous solution by modified red mud, J. Hazard. Mater. 406 (2021), 124678.

[61] H. Masoumi, A. Ghaemi, H. Gilani Ghanadzadeh, Elimination of lead from multi-component lead-nickel-cadmium solution using hyper-cross-linked polystyrene: Experimental and RSM modeling, J. Environ Chem. Eng. 9 (6) (2021) 106579.

[62] A.H. Gedam, R.S. Dongre, Adsorption characterization of Pb(II) ions onto iodate doped chitosan composite: equilibrium and kinetic studies, RSC Adv. 5 (67) (2015) 54188–54201.

[63] M.I.U. Hoque, D.A. Chowdhury, R. Holze, A.N. Chowdhury, M.S. Azam, Modification of amberlite XAD-4 resin with 1,8-diaminonaphthalene for solid phase extraction of copper, cadmium and lead, and its application to determination of these metals in dairy cow's milk, J. Environ. Chem. Eng. 3 (2) (2015) 831–842.

[64] K.Z. Elwakeel, A.A. El-Bindary, E.Y. Kouta, Retention of copper, cadmium and lead from water by Na-Y-Zeolite confined in methyl methacrylate shell, J. Environ. Chem. Eng. 5 (4) (2017) 3698–3710.

[65] Y. Qi, J. Wang, X. Wang, J.J. Cheng, Z. Wen, Selective adsorption of Pb(II) from aqueous solution using porous biosilica extracted from marine diatom biomass: Properties and mechanism, Appl. Surf. Sci. 396 (2017) 965–977.

[66] S. Ai, Y. Huang, C. Huang, W. Yu, Z. Mao, Lead ion adsorption on functionalized sugarcane bagasse prepared by concerted oxidation and deprotonation, Environ. Sci. Pollut. Res. 28 (3) (2021) 2728–2740.

[67] M. Al-Saraj, M.S. Abdel-Latif, I. El-Nahal, R. Baraka, Bioaccumulation of some hazardous metals by sol-gel entrapped microorganisms, J. Non-Cryst. Solids 248 (2) (1999) 137–140.

[68] L. Wang, W.-H. Xu, R. Yang, T. Zhou, D. Hou, X. Zheng, J.-H. Liu, X.-J. Huang, Electrochemical and density functional theory investigation on high selectivity and sensitivity of exfoliated nano zirconium phosphate toward lead(II), Anal. Chem. 85 (8) (2013) 3984–3990.

[69] C. Chen, J. Wang, Correlating metal ionic characteristics with biosorption capacity using QSAR model, Chemosphere 69 (10) (2007) 1610–1616.

[70] J. Roosen, K. Binnemans, Adsorption and chromatographic separation of rare earths with EDTA- and DTPA-functionalized chitosan biopolymers, J. Mater. Chem. A 2 (5) (2014) 1530–1540.

[71] A.A. Galhoum, M.G. Mahfouz, S.T. Abdel-Rehem, N.A. Gomaa, A.A. Atia, T. Vincent, E. Guibal, Diethylenetriamine functionalized chitosan magnetic nano-based particles for the sorption of rare earth metal ions Nd(III), Dy(III) and Yb(III), Cellulose 22 (4) (2015) 2589–2605.

[72] K.Z. Elwakeel, A.A. Atia, E. Guibal, Fast removal of uranium from aqueous solutions using tetraethylenepentamine modified magnetic chitosan resin, Bioresour. Technol. 160 (2014) 107–114.

[73] A.A. Atia, A.M. Donia, S.A. El-Enein, A.M. Yousif, Effect of chain length of aliphatic amines immobilized on a magnetic glycidyl methacrylate resin towards the uptake behavior of Hg(II) from aqueous solutions, Sep. Sci. Technol. 42 (2) (2007) 403–420.

[74] M.O. Abd El-Magied, E.A. Elshehy, E.-S.-A. Manaa, A.A. Tolba, A.A. Atia, Kinetics and thermodynamics studies on the recovery of thorium ions using amino resins with magnetic properties, Ind. Eng. Chem. Res. 55 (43) (2016) 11338–11345.

[75] J. Roosen, J. Spooren, K. Binnemans, Adsorption performance of functionalized chitosan-silica hybrid materials toward rare earths, J. Mater. Chem. A 2 (45) (2014) 19415–19426.